Complex Behavior in the Dynamic Response of a Non-smoothly Forced Mechanical System: Numerical and Experimental Investigations

by

Ashwath Thukaram Kini

Department of Mechanical Engineering and Materials Science
Duke University

Date:_____

Approved:

_____
Lawrie N. Virgin, Supervisor

_____
Robert Kielb

_____
Brian Mann

Thesis submitted in partial fulfillment of the requirements for the degree of Master of Science in the Department of
Mechanical Engineering and Materials Science in the Graduate School
of Duke University
2013

ABSTRACT

Complex Behavior in the Dynamic Response of a Non-smoothly Forced Mechanical System: Numerical and Experimental investigations

by

Ashwath Thukaram Kini

Department of Mechanical Engineering and Materials Science
Duke University

Date:_____

Approved:

_____
Lawrie N. Virgin, Supervisor

_____
Robert Kielb

_____
Brian Mann

An abstract of a thesis submitted in partial
fulfillment of the requirements for the degree of Master of Science in the Department of
Mechanical Engineering and Materials Science in the Graduate School of
Duke University
2013

Abstract

This thesis describes the theoretical and experimental investigations on a non-smooth impacting system consisting of a forced oscillating mass with an impacting barrier, which has the ability to impart energy into the vibrating system. The system is also forced by the means of a sinusoidal excitation using a scotch yoke mechanism. Experiments are conducted to obtain the time delay state-space, time series and Poincaré sections. Bifurcation diagrams are obtained by conducting forward and reverse frequency sweep. The obtained results are compared with expected linear non-impacting behavior and interesting phenomena including hysteresis, multiple-period orbits, transient and sustained chaos are observed. Numerical simulations were conducted and correlations were obtained between the theoretical and experimental results.

Contents

List of Figures

Acknowledgements

First I would like to thank my committee, Dr. Lawrie Virgin, Dr. Robert Kielb and Dr. Brian Mann for taking the time to help me with my research and fine tune my thesis. Special thanks to Dr. Virgin for being a great research advisor, and for all the help and support he has given me during my time at Duke.

I would also like to thank my lab mates Richard Wiebe and Chris George for their help and support with my research, and also for many lively discussions on Nonlinear Systems. In particular, I thank Rick for his help on the mathematical model for impact oscillators and Chris for helping out with LABView and data processing with MATLAB.

I would also like to thank Pat McGuire and John Goodfellow for their assistance with fabrication of the experimental setup and Nikhil Bumb for setting up the hardware for data acquisition using LabVIEW.

Last, but not the least, I would like to thank my family for their constant support during my time at Duke.

1. Introduction

This thesis presents the research done on active impact oscillators, which fall under a special category of non-linear systems known as non-smooth systems. These are systems whose behavior would normally be described by a linear ordinary differential equation with closed form solutions, but the presence of an impacting barrier causes a sudden reversal of the velocity which acts as a non-linearity. This results in the system response being unpredictable by means of the various tools of linear theory available to us. Non-smooth impacting systems are found in a lot of real life machinery such as rattling gear pairs, vibration absorbers etc.

Determination of the system response for an impacting system is quite important since it may adversely affect the life of the system. Generally any vibrating system is designed by assuming the response to be linear and ensuring the operating conditions are far from the resonance i.e. the condition when the operating and natural frequencies are equal. Once the operating conditions have thus been decided, the part is designed by a standard fatigue analysis using a modified Goodman Diagram and the S-N curve for the material.

But it is possible that improper design might result in impacts, and the resulting nonlinear behavior might shift the location of the resonant peak, present multiple coexisting solutions for a certain operating frequency resulting in hysteresis, etc. This would drastically reduce the life of the part resulting in premature failure.

The future sections present a complete discussion on the types of impact oscillators and the various tools available today for analysis.

1.1 Impacting Systems and Grazing Bifurcations

One of the simplest impacting systems is the unforced impacting linear oscillator, a good example of which is a bouncing ball. The behavior, though nonlinear is extremely simplified since the impact is described by a simple coefficient of restitution (C.O.R) model. Some other examples are an unforced impacting pendulum, an unforced spring-mass-damper system impacting a wall, etc. Although non-linear, such systems can exhibit only simple behavior because they are unforced.

A more complicated system would be a forced impacting linear oscillator, where the system is excited by an external forcing with a velocity reversal at the location of the barrier. This system has been the subject of extensive study both theoretically and experimentally, in various forms.

One of the most important theoretical findings in this area was by Nordmark in [1] for the case of a forced oscillator. The mechanism of transition from non-impacting to an impacting orbit by changing a parameter was studied and the term "grazing bifurcation" was coined and the critical value of the system parameter was termed as grazing point. A map was derived to characterize the behavior of the attractor at the grazing point which has later come to be known as the Nordmark Map. Other notable

work in this area to determine the system response for non-smooth systems includes [2] and [3].

In the area of experimental research on impact oscillators, quite a large number of systems have been studied with different parameters being varied to achieve grazing. Thompson and Ghaffari [4] explore the dynamics of a spring –mass-damper system and observed interesting behavior such as period doubling cascades. The ratio of parameter values where period doubling occurs was found to agree with Feigenbaum's analysis, found in any text such as Strogatz [5].

Another interesting system is a forced impacting pendulum as opposed to a linear oscillator. Since the equations of motion governing a pendulum are already nonlinear, lot of interesting behavior is observed. Piiroinen et al [6] and Bayly et al [7] conducted studies on a pendulum where the barrier was set at a fixed location in the oscillation range of the pendulum. At grazing, chaotic behavior and period doubling cascade were observed. Good correlation was also observed with the Nordmark map. More recent work by Davis & Virgin [8] determines the response to a pendulum forced only by an impacting surface, and interesting results contrary to common knowledge are obtained.

1.2 Passive Impact vs. Active impact

An important characterization of a system is the type of impact. The most generalized form of an impact oscillator would be governed by the following set of equations as described by Pring & Budd in [9]:

$$m\ddot{x} + c\dot{x} + kx = F\sin\omega t, x > x_0 \tag{1.1}$$

$$\dot{x}_+ = r\dot{x}_- + V,\ x = x_0. \tag{1.2}$$

The reset law includes a coefficient of restitution, r and energy addition into the system, V. The case where $V=0$ is the one in which the impact is a pure rebound and is known as passive impact. Here, only the C.O.R. dictates the rebound velocity of the system.

The case where $V>0$ is known as an active impact oscillator, i.e. at the time of impact additional momentum in imparted to the mass. The major difference between active and passive impact is the system behavior at grazing. With active impacts it can be seen that depending on the value of V, the rebound velocity can actually be quite higher than the velocity prior to impact; hence a zero velocity impact can trigger a high velocity rebound. This results in interesting behavior at the grazing point as compared to a passive impact.

Another way to incorporate the impact is to model the system as piecewise linear with a value of stiffness k_1 below certain threshold amplitude, and a much higher stiffness k_2 above the threshold as in [10]. This model is useful for a system where the

impacting wall is not rigid, and undergoes certain compression upon impact. Hence the stiffness k_2 would be the compressive resistance of the barrier. For the purpose of this research, the impacting wall is considered rigid hence eqns. (1.1) and (1.2) are used.

Although extensive research has been done over the past few decades on determination of the behavior of impact oscillators, most of the work has been limited to passive impact. Very little literature exists that venture to quantify an active impact oscillator.

1.3 Motivation

The motivation for this research is the numerical analysis by Pring & Budd in [9]. This paper examines a simplified model that is aimed to simulate the behavior of pinball machines, which are complex dynamical systems with 2 degrees of freedom. The pinball is forced by shaking the pinball table, and impact occurs when the ball hits the bumpers on the table. The bumpers have magnetic triggers that are turned on during impact which kicks the ball upon contact, i.e. momentum is added to the ball at the impact location. Hence, the impact is modeled as active in [9] and the behavior is described using eqns. (1.1) and (1.2). Further, the Nordmark map describing the behavior of the system is also derived.

To analyze the system, a lot of simplifying assumptions are done in [9]. The case that is analyzed is that of vibrations in 1-D, instead of a vibrating mass on a plane. Also,

the excitation is assumed to be a harmonic forcing and the damping is assumed to be linear viscous damping. The rebound is assumed to be taking place instantaneously.

Figure 1. A pinball machine as an example of a complex, 2D active impact oscillator (Source: Wikipedia)

1.4 Scope of the research

The nature of this research is mainly to numerically simulate the response of an active impact oscillator and to experimentally validate the numerical response. Interesting non-linear behavior such as period increment cascades and chaotic response is found by means of bifurcation diagrams, time series, Poincaré sections and state space. A few changes are made to the initial system proposed in [9]. In the analysis presented by Pring & Budd, very high values of damping are used. This is done in-order to reduce the 2-D Nordmark map to a 1-D map. Since the analysis of maps is beyond the scope of this research, much lower, realistic values of damping are used in line with

most mechanical systems. Also, since the forcing will be provided by means of a scotch yoke mechanism available in the Nonlinear Dynamics Lab, the equation of motion is modified accordingly with base excitation as the forcing.

Also, the bifurcation diagrams obtained in [9] have the location of the barrier, x_0 as the parameter. Since the scotch yoke is driven by a motor, it is only logical to use to excitation frequency, ω as the bifurcation parameter since it is difficult to move the barrier in real time. Further, only the stroboscopic bifurcation diagram is used to characterize the response in [9]. In mechanical systems, it is often a convention to plot the bifurcation diagram with the amplitudes shown instead of the stroboscopic Poincaré points since this has more physical meaning. Hence, for the sake of clarity, both types of bifurcation diagrams are plotted.

Finally, the experimentally determined state space is determined in time delay coordinates instead of position-velocity coordinates. Time-delay coordinates generally plot the displacement on x-axis and the displacement delayed by a quarter-forcing cycle along the y-axis. This is a common practice in the case of harmonic forcing, since quarter-delayed displacement closely resembles the behavior of the velocity.

For the experiments, the transducer measures the position and hence velocity is obtained by differentiating the signal. Differentiation tends to amplify the noise especially when an impact occurs; hence by using time-delay coordinates the state space is plotted using much cleaner data.

1.5 Outline of Chapters

Chapter 2 begins with a description of the experimental system, including the forcing mechanism and response measurement system, data post-processing procedure and determination of system parameters. In chapter 3 the equations of motion used for numerical simulation, although quite trivial, are shown for the sake of completeness. Chapter 4 deals with a detailed discussion of the numerical and experimental results obtained for passive impact. In chapter 5, more complex results are discussed where the impact is active now, and interesting nonlinear phenomena are observed. Chapter 6 discusses the possibility of chaos at low amplitude excitation and shows the numerical and experimental results obtained. The thesis is concluded with chapter 7 where a summary of the results obtained is presented and the scope for future research is also explored.

2. Experimental Setup

The details of the experimental setup along with the data acquisition and post-processing methodology are included in this section. A detailed discussion on measurement of the system properties such as natural frequency, damping, etc. is also included in this chapter and this data will be used for numerical simulations in Chapter 3. Also presented are details of the limitations of the measurement system and the excitation system, and how these details were used to finalize the system parameters.

2.1 Experimental setup

For the purpose of this research an experimental setup was designed by Dr. Lawrence Virgin and the author and built by Pat McGuire and John Goodfellow of the MEMS department. The experimental setup consists of a base which is mounted directly on the source of excitation, viz. the scotch yoke mechanism as shown in Figure 2. Fixed on top of the base are the linear oscillating system, the impact mechanism and the measurement setup which are discussed in detail below.

2.1.1 Linear oscillating system

The linear oscillating system is designed as a block of mass with linear springs attached to it. The mass is made of High Density Polyethylene which is light weight, impact resistant and also has high machinability. This block of mass is mounted on top of PASCO slider rails, which have low coulomb friction due to the presence of sealed roller bearings and these rails are directly mounted onto the base. Springs are attached

to the sliding mass, one on each side. The springs are attached with sufficient pretension in the static case, so as to make sure it is in the linear operating region. Although no physical dashpot is present, the inherent dissipation from the system is modeled as damping.

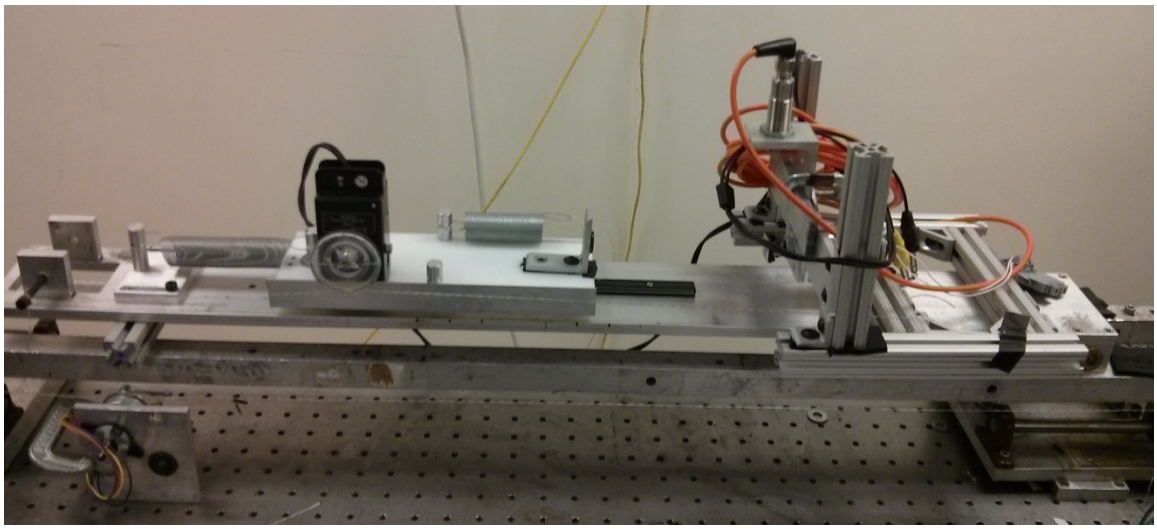

Figure 2. Active Impact Oscillator – Experimental Setup

2.1.2 Active Impact mechanism

A solenoid valve, with a flat Aluminum plate was used as the impact barrier. The solenoid was triggered by means of a photo-sensor which would activate upon sensing the mass at the predetermined barrier location. The photo-sensor is mounted directly on top of the solenoid value, and the solenoid is adjusted such that the stroke of the plunger moves the impact barrier right to the location of the light sensor. If the solenoid valve is turned off, then the system behaves as a passive impact barrier. The linear oscillating

mass has an Aluminum L-block with a rubber button which acts as the point of contact at the barrier. This system is shown in detail in Figure 3.

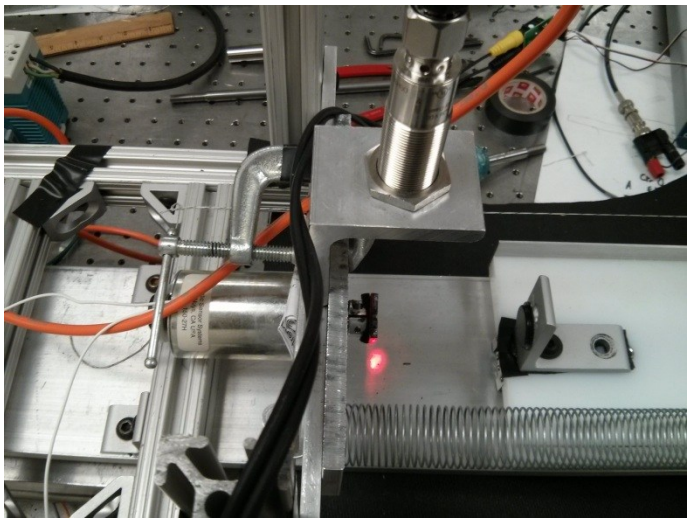

Figure 3. The solenoid value and the light sensor acting as the active impact barrier

2.2 Data Acquisition system

The system response was characterized by measuring the position of the slider using a PASCO rotary transducer at a rate of 50 frames/second. The transducer is mounted on top of the sliding mass, and a thread is passed over the large pulley and fixed on the base at both ends. This setup converts the linear motion of the slider into rotary motion of the transducer, which is measured using a virtual instrument on LabVIEW. The following sub-sections discuss the various results obtained from experimentation.

2.2.1 Bifurcation Diagrams - Amplitude

To measure the bifurcation diagram, the data collected by the rotary transducer was written to a text file. Each data point was written as $(x(t), v(t))$ where $v(t)$ is the excitation frequency of the system. The frequency of the excitation is controlled by the voltage output from LabVIEW which is increased every 4 minutes. The increment in frequency is done such that in the linear regime before impact, the increments are large, and in the nonlinear zone, the increments are small to get a better resolution. From the collected data, post- processing was done in MATLAB to get the extremum.

2.2.2 Bifurcation Diagrams – Poincaré Section

To measure the Poincaré section, physical trigger was created on the motor flywheel using a piece of high reflective tape, which was detected using a tachometer. The output from the tachometer was used as a third data point. Using the rising edges feature in LabVIEW, whenever the reflective tape is detected the tachometer writes a output of 1, otherwise 0. The data is post processed in MATLAB, and by collecting only the points with a tachometer output of 1, the Poincaré section is determined. The existing code for bifurcation diagram- amplitude is modified to incorporate this, and hence both diagrams are obtained from a single run.

2.2.3 Time series and State-space

From the collected data for bifurcation diagrams, the data for the position $x(t)$ is collected individually for each frequency and the time series is plotted. The state-space

for each individual frequency is also plotted. The time-delay coordinates are used, and quarter-lag delay is used for determination of the delayed coordinates. Since it is not necessary that the measurement frequency is a multiple of the quarter-lag, the next highest multiple is used.

2.3 Post-Processing

The data obtained from the experiments was post-processed in MATLAB in order to remove any transients (if present), spurious points, false peaks, etc. Three separate codes were written in order to obtain the necessary output: One for the plotting the bifurcation diagram showing the response amplitude, second for plotting the bifurcation diagram showing the Poincaré points, and the third for time series, state space and delayed Poincaré section.

2.4 System characteristics

2.4.1 Natural frequency

The natural frequency was determined by measurement of the unforced free oscillations by providing an initial displacement to the system. Since the free vibrations occur at the natural frequency, the theoretical curve was plotted to fit the experimentally observed response as shown below in figure 4. From the best fit curve, the natural frequency of the system was found to be 0.94 Hz

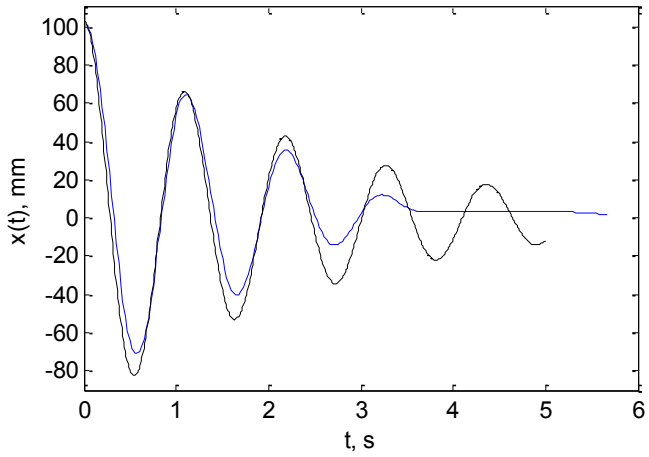

Figure 4. System response to ICs, used to determine the natural frequency and damping (log-dec)

2.4.2 Damping

The damping was measured using two of the popular methods, i.e. log dec method and half power method. But since the system is not lightly damped, the linearized expression for ζ cannot be used. Hence, a best-fit approximation was used for both methods.

2.4.2.1 Log dec method

The damping according to log-dec method was determined by using a value of ζ that gives the best fit for the free decay shown in Figure 4. Using trial and error, a value of $\zeta = 0.052 = 5.2\%$ was determined to be the best fit since it gives good correlation for the first two decay peaks. It is important to note that for further peaks, the amplitude dies down much faster than expected by the theory due to the presence of coulomb friction damping, which becomes prominent at lower amplitudes.

2.4.2.2 Half-power method

The system FRF in frequency domain was measured for the linear case in order to determine the damping by half-power method. The FRF is shown in figure 5 on next page. The best fit was obtained for a value of damping $\zeta = 0.07 = 7\%$

It is interesting to note that the damping estimate from the half-power method is slightly higher than that estimated by the log-dec method. Hence, the actual value of damping used for all further numerical simulations is the average of the two, i.e. $\zeta = 6\%$. Another point worth mentioning is the flat peak at resonance which is uncharacteristic of linear oscillators. This is in fact due to physical constraint of the slider, which has a peak-to-peak stroke of 200 mm. At resonance, the actual amplitude is greater than this value and hence the slider strokes out, thus causing the flat peak.

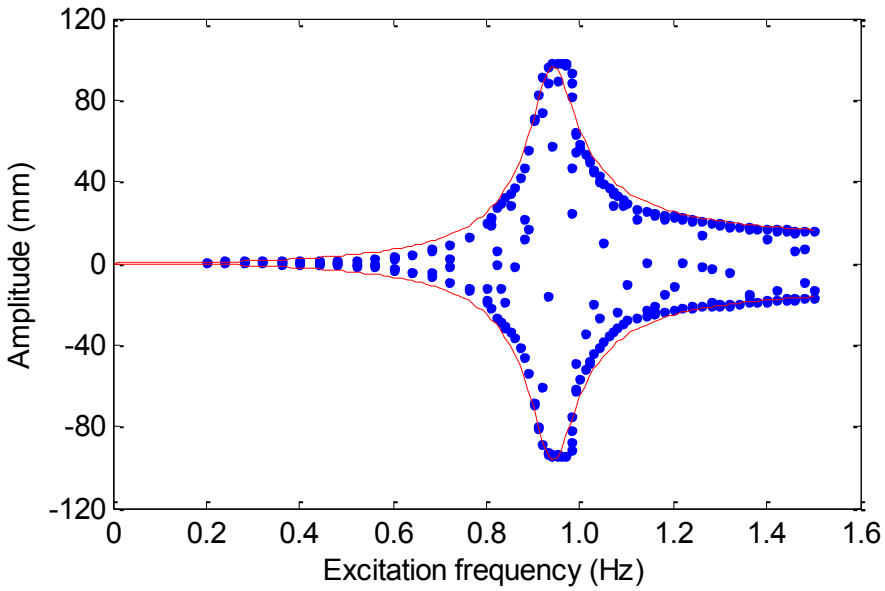

Figure 5. FRF for linear case, excitation amplitude = 10 mm

2.4.3 Coefficient of restitution

One of the most important physical parameters in this research is the coefficient of restitution, since it decides the strength of the non-linearity. A higher value of coefficient of restitution can mean the difference from a simple 1-period impact to chaotic behavior.

The response of the mass is measured, this time with the impact barrier in place. The velocity vs. time graph is plotted as shown in figure 6. By definition, we have the following relation for coefficient of restitution

$$r = \frac{v_-}{v_+}.$$

Hence by taking the ratio of velocities before and after impact, the coefficient of restitution is found to be $r = 0.78$

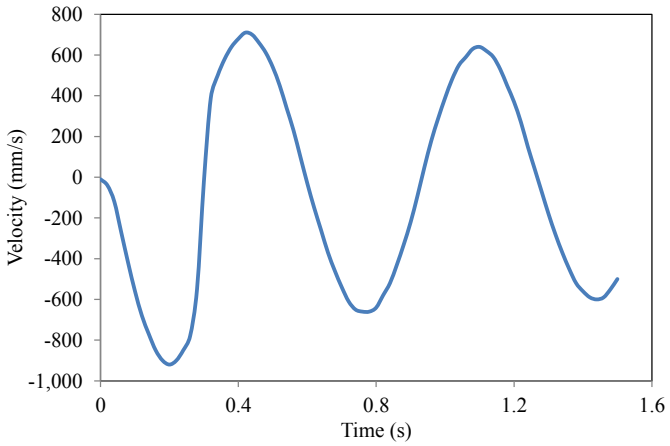

Figure 6. Velocity vs. time for free decay. ICs: Position = 100 mm, velocity = 0

2.4.4 Active Impact - momentum input measurement

Possibly the most important physical parameter of the measurement system is the 'kick' provided by the solenoid to the mass, which manifests in the form of a momentum input as shown in equation (2). For measurement of this momentum input, the solenoid trigger is switched on and a force transducer is used at the location of the L-bar on the mass.

By means of the setup the force of impact vs. time is obtained in LabVIEW as shown in figure 8. Since the momentum added is given by $\int Fdt$, the solenoid kick can be determined. The value thus determined is found to be $V = 0.18\, m/s$.

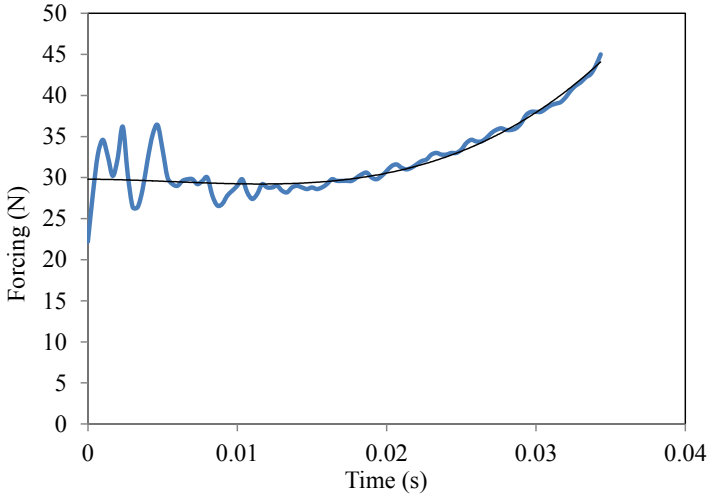

Figure 7. Force vs. time during active impact

The force of impact was also measured using a second method in order to confirm the result obtained above. The system was allowed to oscillate while coming in contact with the impact wall and the solenoid trigger was left on. The position of the barrier was adjusted so that the mass exhibited sustained oscillations due to the solenoid

kick. The experimental state space was plotted and compared with the theoretical value and value of V was varied till a best fit was obtained. Figure 8 below plots the state space for $V = 0.17\ m/s$ which presents a good correlation.

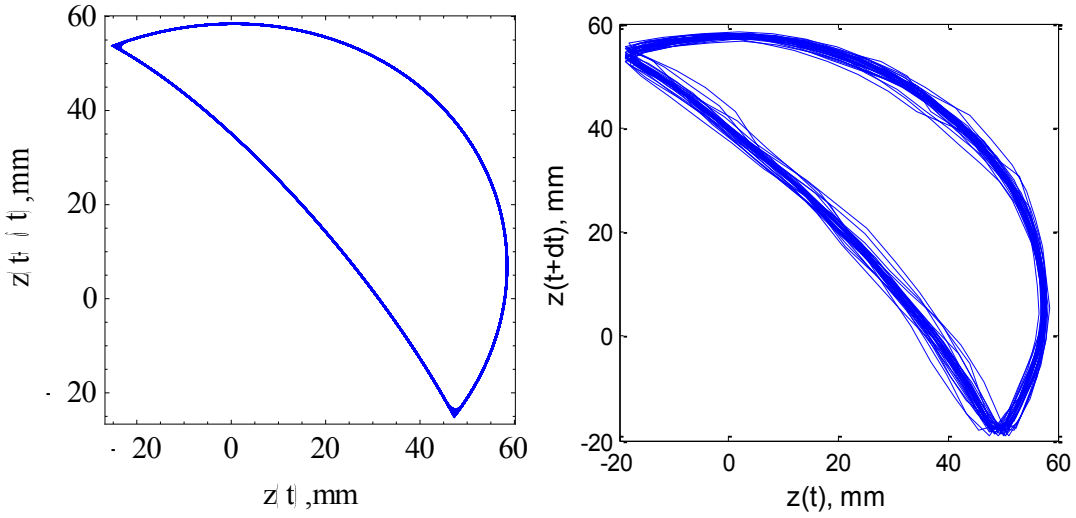

Figure 8. State space for unforced active impact with z_0 = -25 mm. Numerical (left) and experimental (right) show good correlation

2.5 Limitations

The following are the limitations of the experimental measurement system, which in turn decided the values of some of the parameters for numerical simulations in the future chapters.

1. Scotch-yoke mechanism – The mechanism is forced by a motor which is driven by means of a voltage input from LabVIEW. It was observed that at low amplitudes (~ 5-10 mm) the scotch yoke was able to operate up until frequencies close to 1.6 Hz. Hence, most of the experiments are conducted only up to a frequency of 1.5 Hz~1.6 Hz, since the feedback into the scotch-yoke due to impact was very high at higher frequencies.

2. PASCO Slider – the slider used for mounting the oscillating mass has a total stroke of 200 mm peak-to-peak. Hence, considering the value of damping and the amplification factor at resonance, excitation amplitudes higher than 10 mm were not used for experiments.

3. Equations of motion

The equations of motion for the oscillating mass, along with the reset law that determines the velocity after impact, are derived in the following sections of this chapter. Using the system, the grazing points are determined as a function of the barrier location. Before analyzing the equations of motion, it is important to note the following assumptions:

1. The vibrating mass is rigid, and doesn't undergo any deformation during impact
2. The coulomb friction from the sliders is negligible
3. Impact is instantaneous and perfectly elastic
4. The reaction time for the solenoid is zero, and the kick is instantaneous
5. The springs operate within the linear range, i.e. Hooke's law is satisfied
6. Scotch yoke excitation is purely harmonic

3.1 Equations for the oscillating mass

From basic linear vibration theory, the equations of motion for a vibrating mass undergoing base excitation is given by the following relation:

$$\ddot{x} + 2\zeta\omega_n\dot{x} + {\omega_n}^2 x = 2\zeta\omega_n\dot{y} + {\omega_n}^2 y \tag{3.1}$$

where:

- x = Position of the vibrating mass measured from equilibrium
- ζ = Critical damping ratio
- ω_n = Natural frequency

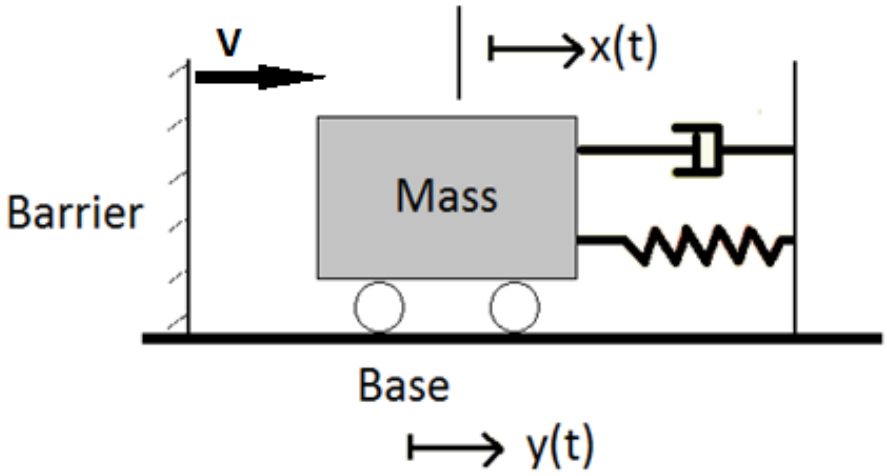

Figure 9. Schematic of the spring-mass-damper system shown with the excitation source y(t) and the active impact V

- y = Excitation given to the base.

Assuming a sinusoidal excitation, the forcing can be expressed as

$$y = y_0 \cos(\omega t - \tfrac{\pi}{4}). \tag{3.2}$$

Note that a phase lag of $\pi/4$ has been added to the forcing. This is done in order to get the same Poincaré section as the reflective strip. By adding the correct phase, the experimental and theoretical Poincaré sections will agree both qualitatively and quantitatively.

Further modification is made to the equation of motion in order to better simulate the experimentation. Equation (3.1) above determines the absolute position of the mass, whereas the experimental result obtained is the position of the mass relative to the base, i.e. $z = x - y$, where z is the relative motion of the mass. Making the substitution in equation (3.1) we get

$$\ddot{z} + 2\zeta\omega_n\dot{z} + {\omega_n}^2 z = -\ddot{y}. \tag{3.3}$$

Substituting for y from (3.2), we get the following:

$$\ddot{z} + 2\zeta\omega_n\dot{z} + {\omega_n}^2 z = \omega^2 y_0 cos\left(\omega t - \frac{\pi}{4}\right). \tag{3.4}$$

It is important to note that (3.4) completely describes the motion of the oscillating mass for $z > Z$, i.e. for any point in the state space not at the location of the impact.

3.2 Reset law for impact

The equation governing the velocity reset is given by the relation

$$\dot{z}_+ = -r\dot{z}_- + V \; at \; z = Z \tag{3.5}$$

where

- r = coefficient of restitution
- V = momentum added to system (fo active impact)

(3.5) is known as the reset law, and this is the non-linearity introduced in the system. (3.4) and (3.5) together describe the behavior of the system.

3.3 Grazing points from linear analysis

If the linear case be considered, assuming a solution of the form $z = z_0\cos(\omega t - \phi)$ and substituting back in the (3.4) it is possible to break down the values of z_0 and ϕ into the frequency domain, and the following expression is obtained for the amplitude:

$$\frac{|z_o|}{y_0} = \frac{\left(\omega/\omega_n\right)^2}{\left[\left(1-\left(\omega/\omega_n\right)^2\right)^2 + \left(2\zeta\omega/\omega_n\right)^2\right]^{0.5}} \tag{3.6}$$

In the above expression, if the location of the barrier is substituted, then the value of the frequency at which the mass will graze the barrier can be determined. Although this linear analysis is trivial, it gives a closed form expression for onset of grazing which can later be used to correlate with experimental findings.

For chapters 4 and 5, the experiment is conducted for a value of $Z = -60mm$. Using the relation (3.6) the grazing points are determined to be $\omega = 0.887\,Hz$ for the upsweep and $\omega = 0.995\,Hz$ for the down-sweep.

4. Passive impact

This chapter describes the behavior of the system in the case of passive impacts. We begin with the frequency sweep depicting the global extremum of the position followed by a Poincaré section. Both the experimental and theoretical results are presented here.

4.1 Bifurcation diagram- amplitude

The bifurcation diagram is presented here for excitation amplitude of 10 mm, with the barrier present at -60 mm. The frequency is swept up from 0 to 1.5 Hz and then a down sweep is also conducted in order to capture co-existing solutions. Figure 10 (a) depicts the numerical solution, whereas 10(b) shows the experimentally obtained analog. The upsweep is shown in blue and the down-sweep in black color. The correlation is pretty good between the two results.

For a frequency range of 0 to approximately 0.9 Hz, the behavior is linear and takes the shape of the linear FRF. At $\omega = 0.887\ Hz$, as discussed in section 3.3 grazing occurs and nonlinear behavior sets in. For $\omega = 0.9 - 1.3\ Hz$, the system responds as a period-1 impacting attractor. As the frequency is swept beyond 1.3 Hz, the nonlinear attractor dies off and the systems returns to the linear response as described by the FRF.

For the down-sweep, the linear behavior is retained until $\omega = 0.995\ Hz$ and then grazing occurs. The system jumps to the nonlinear, single-period impacting attractor and continues along until $\omega = 0.9\ Hz$, at which point it returns to the linear attractor.

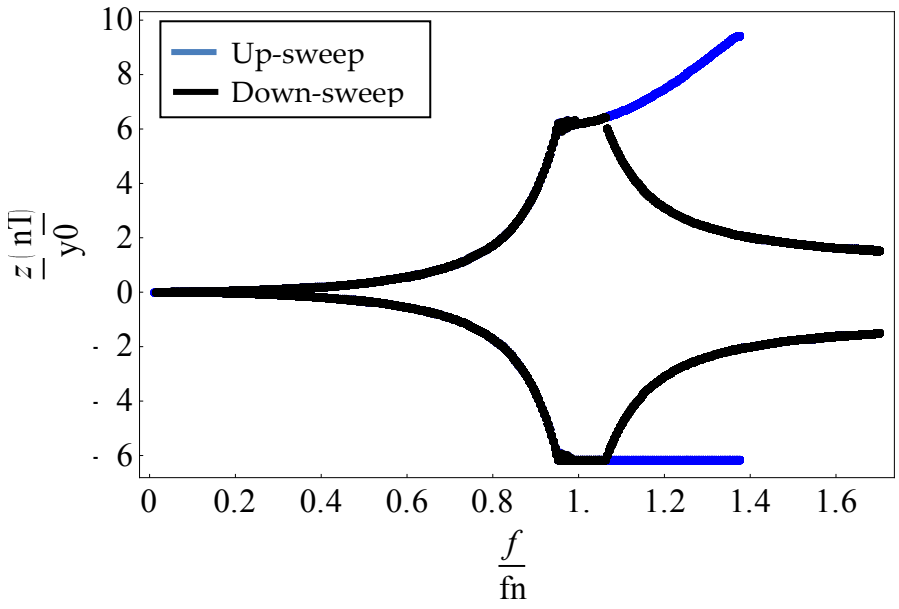

(a) Numerical results

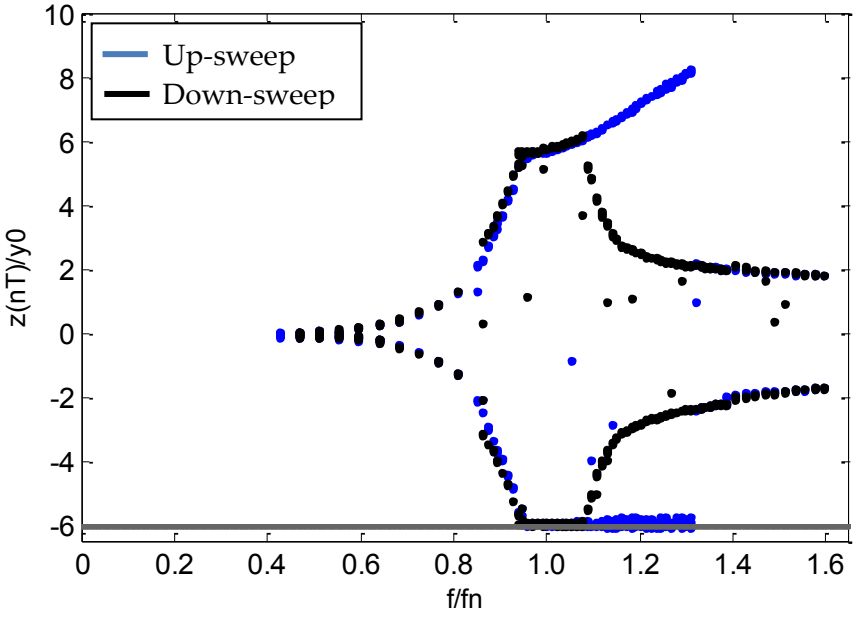

(b) Experimental results

Figure 10. Bifurcation diagram showing the response amplitude for passive impact with y_0=10 mm, z_0=-60 mm (a) Numerical (b) Experimental

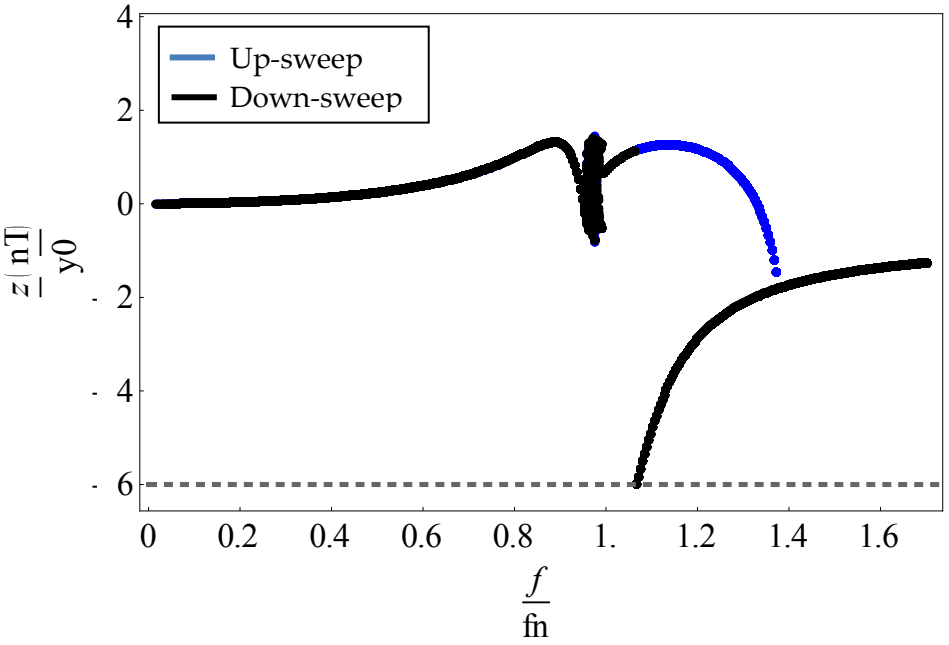

(a) Numerical results

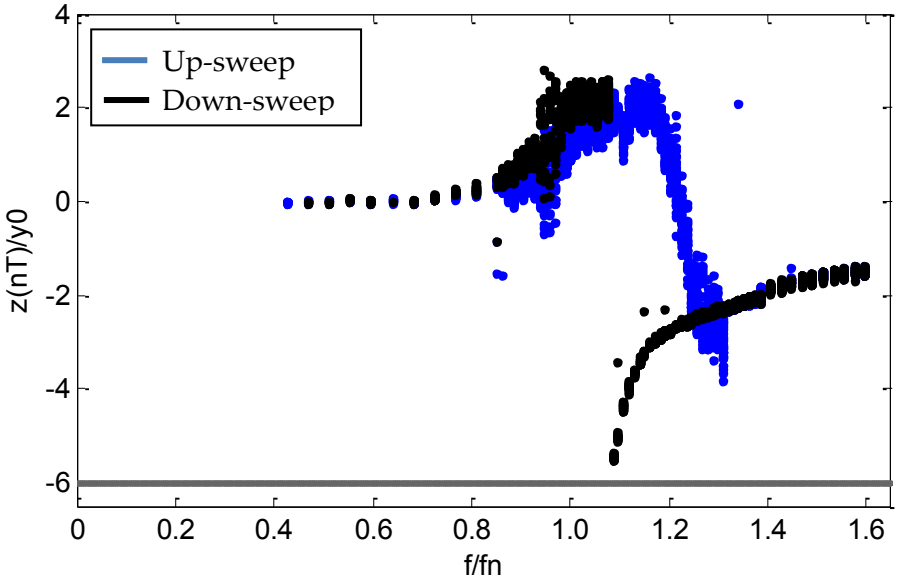

(b) Experimental results

Figure 11. Bifurcation diagram showing the Poincaré section for passive impact with y_0=10 mm and z_0=-60 mm (a) Numerical (b) Experimental

The experimental bifurcation diagram displaying the response amplitudes shows a few stray points. This is due to the nature of the algorithm used to determine the peaks, which checks for the turning points for the data obtained and hence identifies the points with a zero derivative. It is possible for false peaks to creep into the data due to high sampling rate, etc. and show up as stray points. Although a filtering algorithm is used to filter a large portion of the stray data, a few points still remain.

4.2 Bifurcation diagram – Poincaré

The next image is the more frequently used bifurcation diagram showing the Poincaré section. This is standard procedure for forced non-linear systems [11], and following the normal convention the Poincaré section is Stroboscopic. The sections shown here is stroboscopic, i.e. the position of the slider at each integral multiple of the excitation frequency is used to construct the diagram. This method is useful to determine the periodicity of the response. However, a disadvantage is that sub-harmonics are not shown, which can be seen in the bifurcation diagram- amplitude.

There is a sudden shift in the location of the strobe point near the natural frequency. This is actually expected since the phase shift of response as one passes through the resonant peak is a known behavior in linear systems, and this has carried over to the non-linear system as well.

4.3 Time delay and time series

The time delay graphs and time series, including the Poincaré sections, have been shown in appendix A, Figures 18 through 23.

Although most of the response observed is a period one attractor, some interesting behavior is seen at the grazing point. Although not clearly seen in the bifurcation diagram presented above, a small region of chaos exists from $\omega = 0.9\,Hz$ and $\omega = 0.92\,Hz$. This can be seen from the state space shown in Figure 18. One of the most interesting behaviors seen is the Poincaré section for the chaotic region as shown in Appendix B figure 34. The Poincaré section exhibits the well-known "finger" structure which correlates the previous findings in literature.

4.4 Hysteresis and basins of attraction

As can be seen from the bifurcation diagrams presented above, multiple solutions exist for a frequency range of approximately 1 Hz to 1.3 Hz. The system exhibits hysteresis over quite a wide range of operating frequencies, and the responses are extremely different from each other. One is a linear solution where the system oscillates at quite low amplitudes, whereas the second coexisting solution is a single period impacting oscillator whose amplitude is much higher than the linear solution.

The basins of attraction for three different excitation frequencies within the hysteresis region are shown in figure 12. For $f = 1.05\,Hz$ majority of the ICs tend to settle onto the nonlinear 1-period impacting attractor, since the linear attractor is just

born at this frequency. From fig. 12(b) it is seen that for $f = 1.15\ Hz$ a larger portion of the IC space is settling onto the linear attractor. Finally at $f = 1.3\ Hz$, a large portion of the ICs are attracted to the linear attractor. The plots shown are numerical basins, experimental basins have not been determined

This behavior is typical of systems exhibiting hysteresis. When a second attractor is born, it tends to attract a very small portion of the IC space. As the parameter is further changed, a larger portion of the ICs tend to get attracted to the second attractor. This continues till the end of the hysteresis, when a large portion of the ICs settle onto the second attractor.

As can be seen, non-linear behavior is observed in the case of a passive impact and chaotic response is observed only near the grazing point. There is also some hysteresis present, which is typical of a nonlinear system. But a lot of interesting behavior such as period doubling cascades, chaos over a large parameter range, etc. is not observed. In the next chapter, the case of the active impact is explored and the difference in behavior from the passive case is discussed.

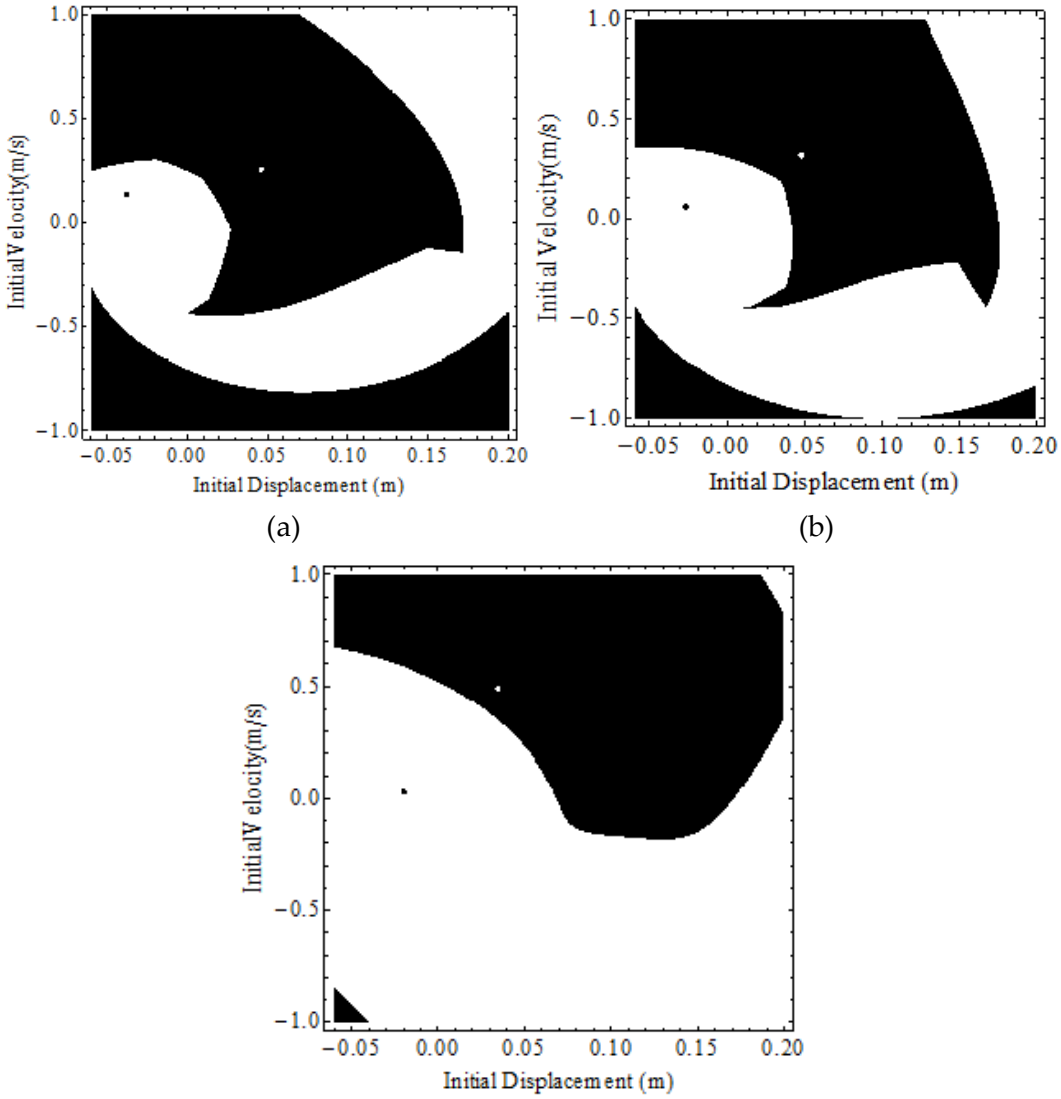

Figure 12. Numerical basins of attraction for passive impact, y_0=10 mm, z_0 = -60 mm at (a) f=1.05 Hz (b) f=1.15 Hz and (c) f=1.3 Hz

5. Active impact

This chapter describes the behavior of the system in the case of active impacts. For the sake of comparison, the exact same excitation amplitude as in Chapter 4 i.e. $y_0 = 10\,mm$ is used. The system behavior is characterized by first plotting the bifurcation diagram – Amplitude and Poincaré and then a discussion of the behavior for various frequencies ensues.

5.1 Bifurcation diagrams

Figures 13 & 14 show the numerical and experimental bifurcation diagrams for the active impact. As can been seen, the nonlinear behavior upon grazing is richer and a period incrementing cascade is seen. Upon impact, the system immediately shifts to a period-3 orbit and this behavior persists for about 0.2 Hz, after which the stable orbit shifts to a period-4. This period doubling continues and 5-period and 6-period orbits are born. More detailed description of the period doubling is given in the next section.

At an excitation frequency of about 1 Hz, hysteresis is born from where on the reverse sweep gives a linear oscillator as the stable attractor and the forward sweep produces a period-5 oscillator. At higher frequencies, the period-5 orbit then gives way to a period-4 and then finally to a single period attractor at about 1.03 Hz. From here on, a large hysteresis region exists up to a frequency of approximately 1.5 Hz. The difference from a passive impact is clearly seen here, since multiple period orbits are born immediately upon impact.

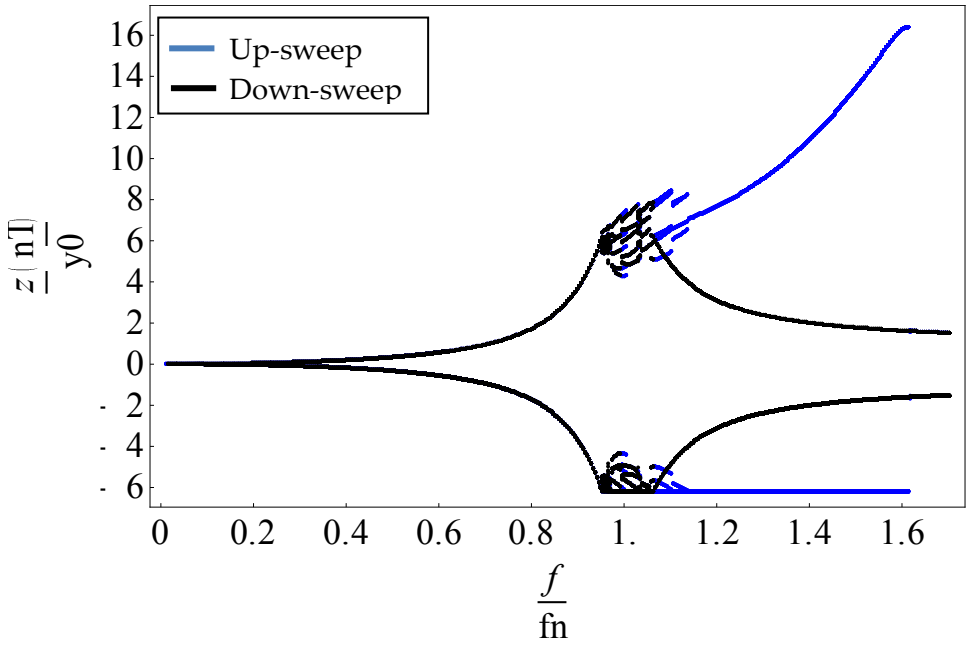

(a)

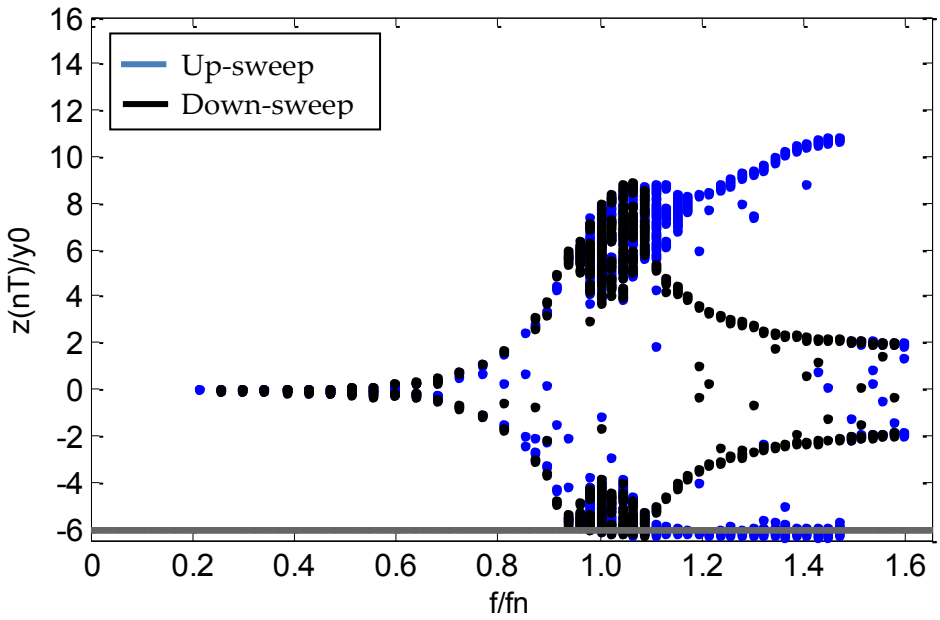

(b)

Figure 13. Bifurcation diagrams showing the response amplitude for active impact with y_0=10 mm and z_0=-60 mm (a) Numerical (b) Experimental

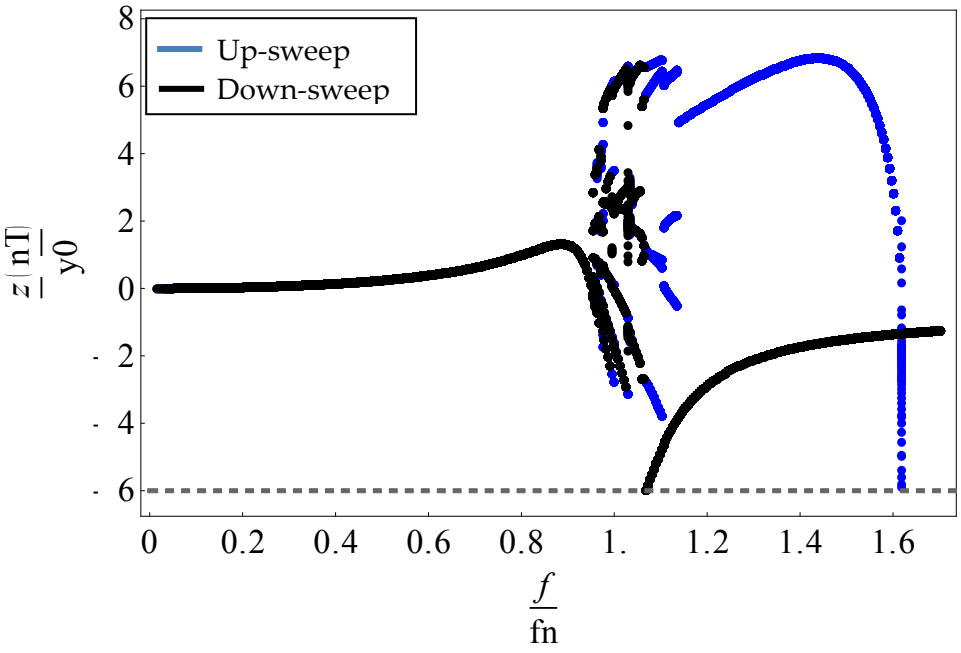

(a)

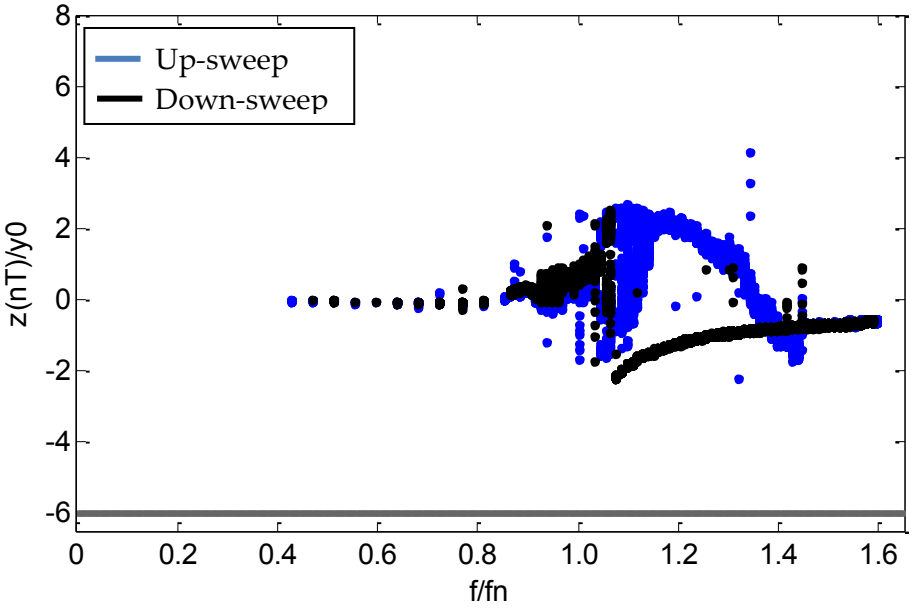

(b)

Figure 14. Bifurcation diagrams showing the Poincaré section for active impact with y_0=10 mm and z_0=-60 mm (a) Numerical (b) Experimental

5.2 Period incrementing cascade

Figure 15 below shows the bifurcation diagram – Poincaré for f = 0.85 to 1.1 Hz. The highly nonlinear behavior is clearly seen. Multiple period orbits separated by regions of chaos are observed, with multiple regions of hysteresis.

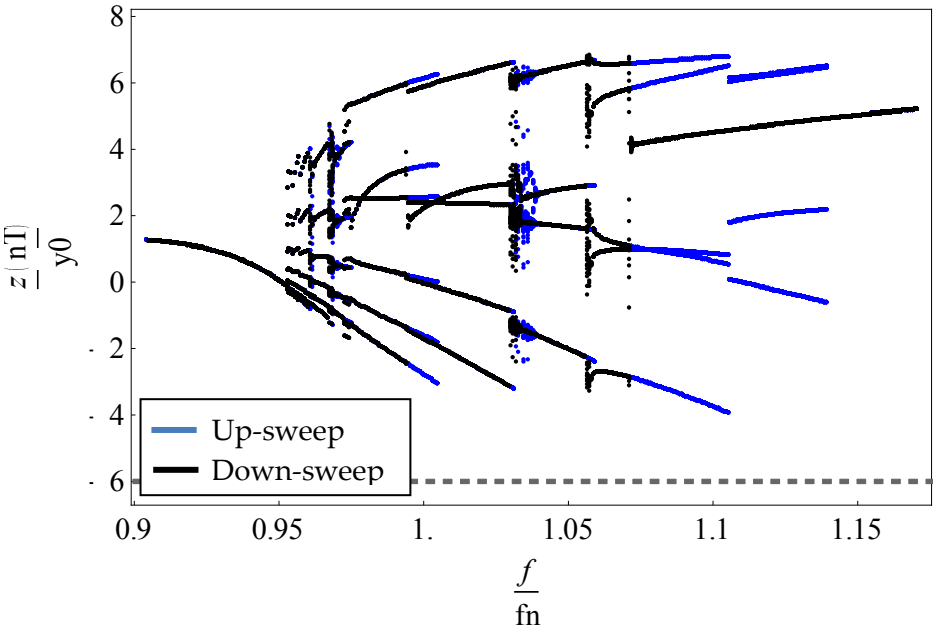

Figure 15. Numerical bifurcation diagram showing Poincaré section for active case with y_0=10 mm, z_0=-60 mm and f=0.85 Hz to 1.1 Hz.

At grazing point, a high period orbit is born and as the frequency is increased, the attractor rapidly decreases in periodicity for a small window until about 0.93 Hz where it settles down to a 6-period attractor. As frequency is further increased, the orbits slowly reduce to 5-period, 4-period and so on until the nonlinear solution dies away and only the linear solution exists.

Also interesting to note are the small windows of chaotic behavior occurring on multiple occasions at $f \approx 0.91\ Hz, 0.96\ Hz\ and\ 0.99\ Hz$ and the chaotic windows act as

separators for the periodic orbits. Such behavior is also reported by Pring et al in [9] although the system analyzed in that case was for high damping.

5.3 State space and time series

From the figures 24 to 28, the periodicity of the response is quite apparent for different operating frequencies. A point worth mentioning is the slight difference in results obtained from the experimental and numerical simulations. This is due to a large number of reasons. Firstly, the impact which occurs at high velocities creates very strong vibrations which modify the behavior of the scotch yoke forcing and it no longer is perfectly sinusoidal. Also, the light sensor has a large spread due to which the position of the barrier becomes a range instead of a single point. Further, the solenoid has a certain response time, although numerically that is assumed to be instantaneous response. This response time causes distortion of the data at high velocity impacts.

5.4 Basins of attraction

By comparing the bifurcations diagrams in fig. 14 with the zoomed in diagram in fig. 15, it is clearly seen that multiple regions of hysteresis are present. Certain solutions present themselves in fig. 15 which isn't obtained in fig. 14. This is because of the nature of the algorithm used to plot the diagrams. The numerical integration is carried out for a certain value of frequency, and the Poincaré points are obtained. Then the frequency is incremented to the next value, and the integration is redone using the solutions obtained for the previous run as the ICs. This helps to cut down the transient time and makes the

algorithms faster. But this also means that each bifurcation diagram can only show two solutions, one corresponding to the upsweep and the other, the down sweep.

Hence, additional attractors and hysteresis are seen in fig. 15 during the down sweep. The basins of attraction for a few values of frequency are shown in fig. 16 below

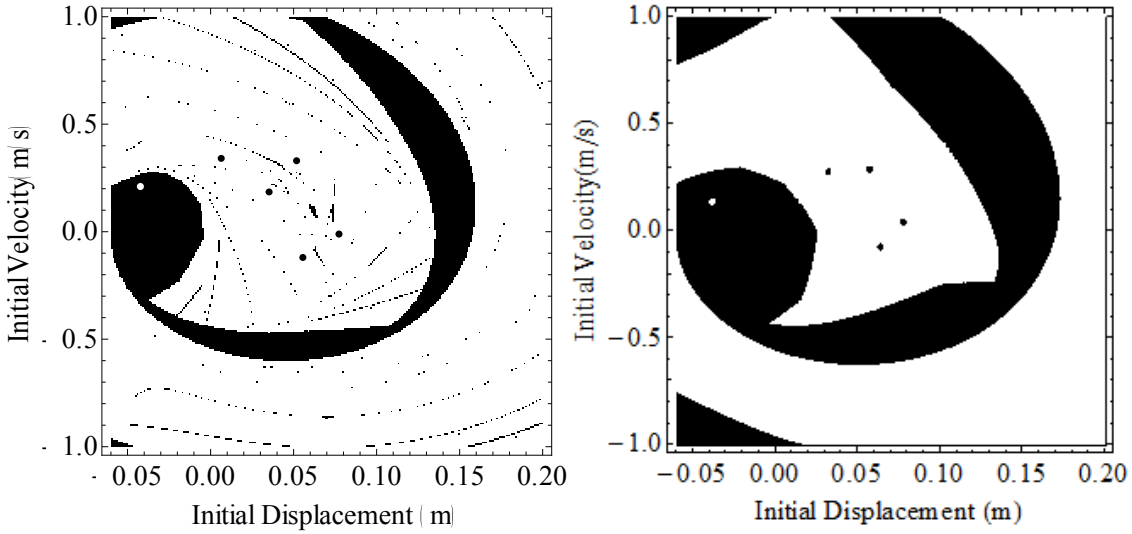

(a) (b)

Figure 16. Numerical basins of attraction for active impact with y_0=10 mm and z_0=-60 mm for (a) f = 1.015 Hz and (b) f=1.05 Hz.

The basins are seen to have complicated shapes with 16 (a) even displaying fractal basin boundaries. In (a), the coexisting attractors are a period-5 and period-1 impacting orbits. In (b) the period-5 attractor gives way to a period-4 attractor, but the period-1 attractor remains the same. A larger portion of the IC space is seen to settle onto the period-1 attractor as expected.

For the case of active impact, much more interesting behavior is seen such as period incrementing cascades with chaotic windows, fractal basins, etc. The next chapter explores the response to low excitation amplitudes where the momentum addition into

the system by the solenoid overpowers the forcing due to base excitation. The stronger the solenoid-kick relative to forcing, the more pronounced the effect on system response at grazing.

6. Chaos

In the present section, numerical and experimental results are shown for the case of low excitation amplitudes. Since the aim of this research is to investigate interesting behavior for active impacts, the passive case is not discussed here.

6.1 Low amplitude oscillations

In chapters 4 and 5, the system response to excitation amplitude of 10 mm has been discussed. This value of excitation amplitude was chosen so as to utilize the complete stroke of the slider mechanism. For $z_0 = 10\ mm$, the amplification at resonance was such that the system response had an amplitude close the maximum possible stroke.

Although this has given us some interesting insight into the behavior of the system, more interesting and complicated non-linear behavior is observed at low excitation amplitudes. This is because the system behavior near grazing depends heavily on the ratio of the solenoid-kick to the excitation amplitude. This is depicted in the figure 17 below, where the passive vs. active impact for two extreme excitation amplitudes have been plotted in the form of state space. Since the point about to be made is regarding the velocity, figure 15 shows the state space as velocity vs. position instead of the time-delay graphs used throughout the rest of this thesis.

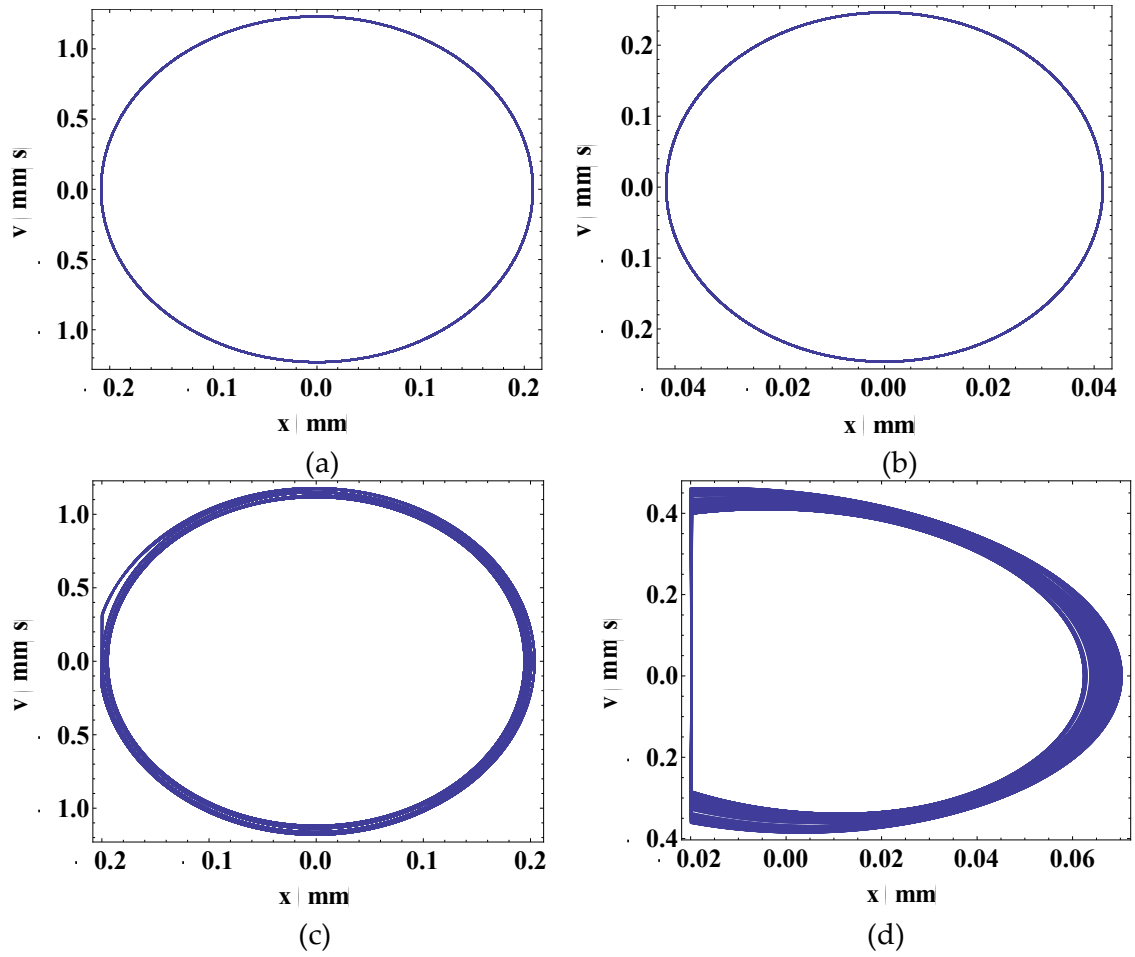

Figure 17. Numerical state space for passive impact and active impact for different amplitudes (a) Linear, z_0 =25 mm (b) Linear, z_0 =5 mm (c) Active grazing, z_0 =25 mm and (d) Active grazing, z_0 =5 mm

In the above graphs it should be noted that the passive impact looks similar to the linear case. This is because the results shown are at the grazing, where the state space is just coming in contact with the barrier. It is clearly seen that the response in 17 (d) for the low amplitude case is much more interesting as compared to that in 17 (c) for high amplitude.

This is attributed to the size of the state space and the max velocity attained by the oscillating mass which increases linearly with the excitation amplitude. Recalling that the momentum added to the system is 0.18 m/s during active impact and taking the ratio of the momentum added to the max velocity obtained, it can been that in the case of 17 (c) the ratio is quite small, whereas it is almost a ratio of 1 for 17 (d). Hence, it is seen that active impact makes great difference in the case of low amplitude excitation.

6.2 Excitation amplitude = 7 mm

The bifurcation diagrams – both showing the amplitude and the Poincaré section were collected by running a frequency sweep of the system from 0 to 1.6 Hz as shown in figures 18 and 19 below. The response is extremely chaotic for a large portion of the frequency range. For $\omega = 0\ to\ 0.9\ Hz$, the response is linear as expected. As soon as grazing occurs, the response becomes highly chaotic, and the size of the chaotic attractor grows with an increase in the amplitude.

At $\omega = 1.1\ Hz$, the chaotic response gives way to period-10 response and further down close to 1.15 Hz the response changes to a period-1 impacting oscillator. The linear behavior is completely lost once the grazing point is crossed. During the reverse sweep, similar behavior is observed. At $\omega = 1.25\ Hz$, the period-1 attractor gives way to a period-10 which close to 1.5 Hz again gives way to the period-10 attractor. As can be seen, a region of hysteresis exists between 1.15 Hz and 1.25 Hz. The corresponding state space and time series have been shown in Appendix A figures 29 through 33.

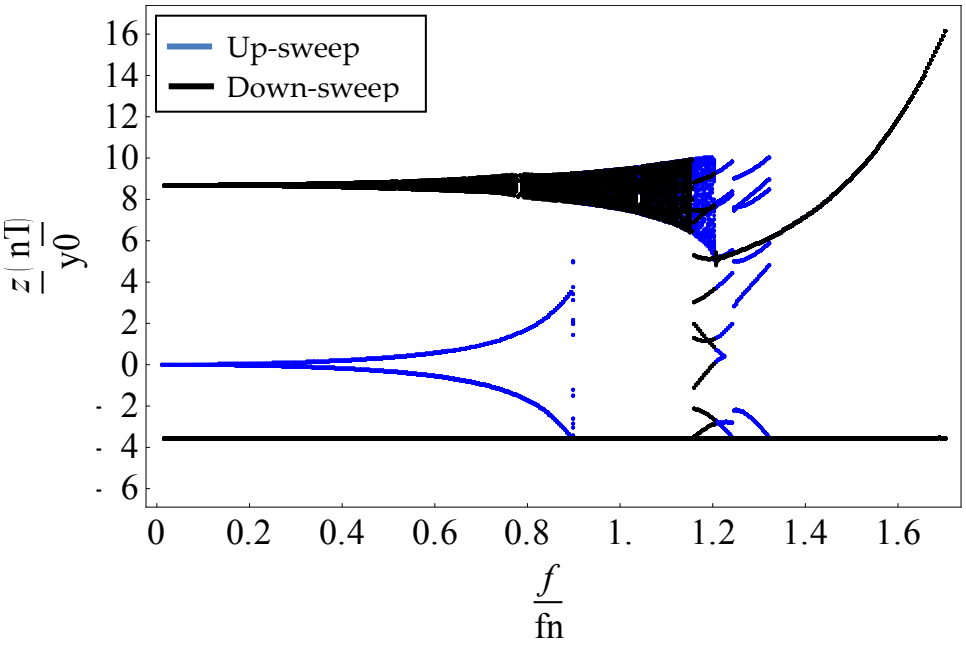

(a)

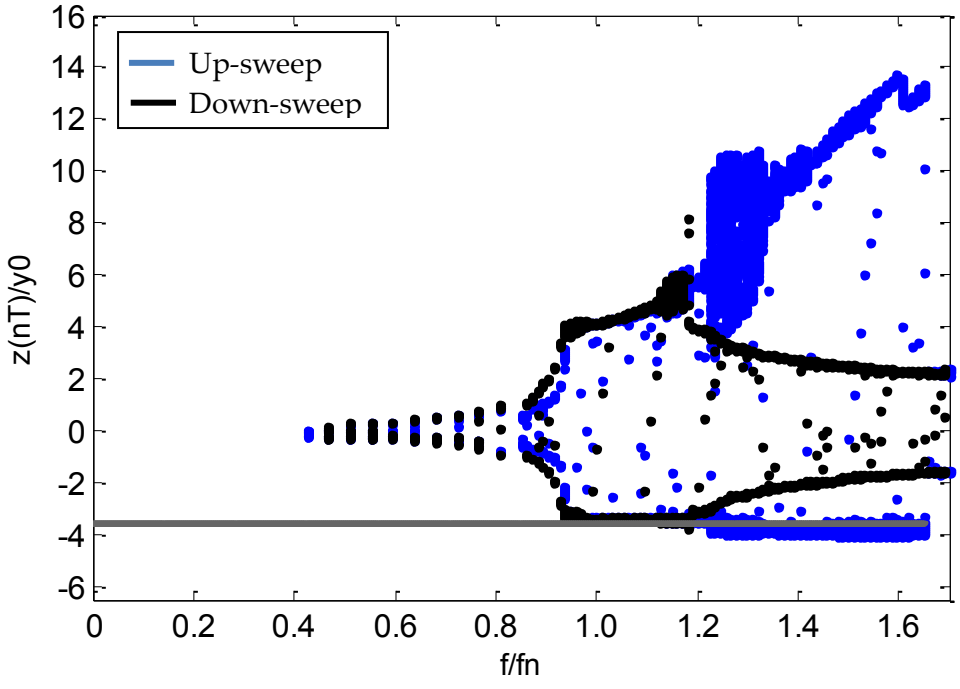

(b)

Figure 18. Bifurcation diagram showing the response amplitude for active impact with y_0=7 mm and z_0=-25 mm (a) Numerical and (b) experimental

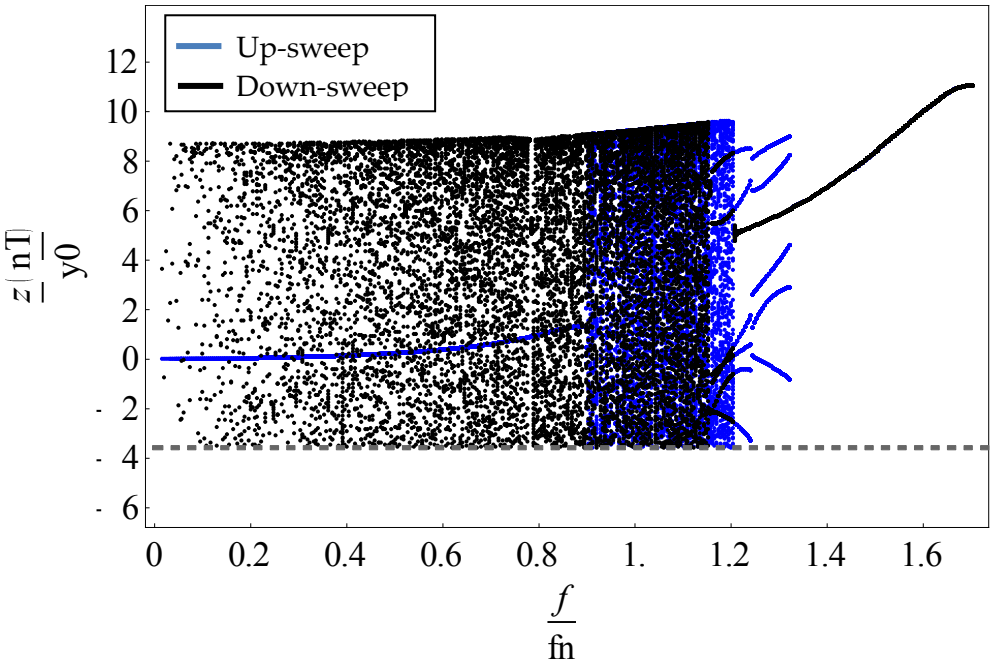

(a)

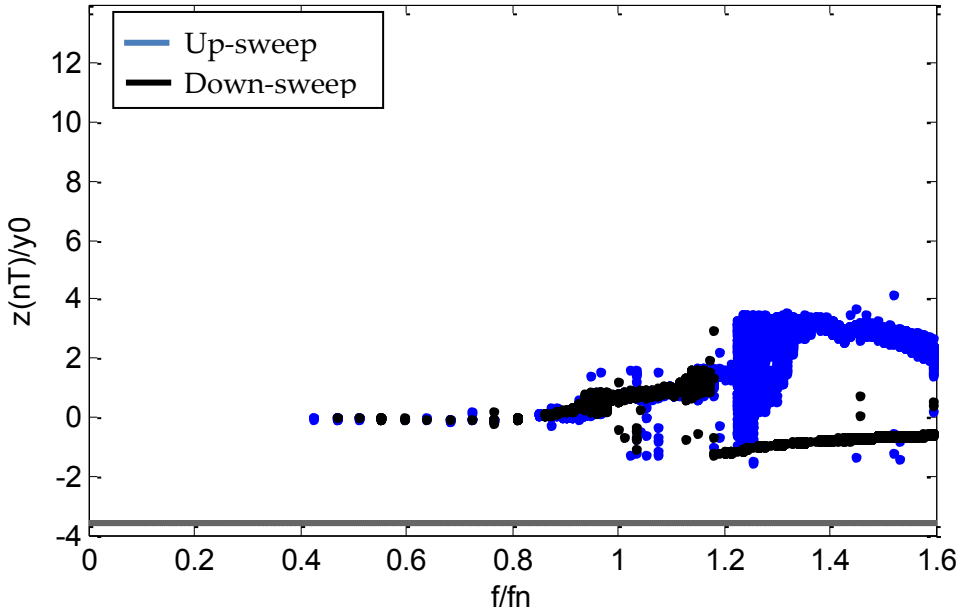

(b)

Figure 19. Bifurcation diagram showing the Poincaré section for active impact with y_0=7 mm and z_0=-25 mm (a) Numerical and (b) experimental

An interesting behavior is seen during frequency down sweep -the system has an attractor even when the forcing is turned off. At $f = 1\ Hz$ the chaotic orbit is born, as is evident from both the bifurcation diagrams. As the frequency is swept down, the chaotic attractor continues to co-exist along with the linear attractor. At $f = 0\ Hz$, although the linear attractor dies down, the chaotic attractor gives way to a period-1 impacting attractor.

This behavior can be expected for the case when the solenoid kick is large relative to the forcing amplitude. In such a case, just the kick is sufficient to generate a stable steady-state impacting orbit. Looking back to section 2.4.4., the kick from the solenoid was in fact measured by a similar experiment.

There is some mismatch between the numerical and experimental bifurcation diagrams. This is mainly because the experiment and numerical simulations lock onto different solutions during the sweep. By running the program with different ICs it is possible to get perfectly matching behavior.

7. Conclusions and Scope for Further Research

This thesis presents the work done on active impact oscillators and shows some of the results in the forms of bifurcation diagrams, time series and state space. Numerical models are developed and experiments are conducted to determine the behavior of the system. Although the work done has been quite intensive, there is still much scope for further experimental and theoretical investigations. The following sections discuss some of the results and the scope for future work.

7.1 Conclusions

From this research, it has been successfully proved that impact oscillators can display a wide range of nonlinear behavior including period incrementing cascades, chaos and hysteresis. Further, the difference between active and passive impact, specifically the effect of addition of momentum at the grazing point has been explored. A numerical simulation model was developed in Mathematica for time integration of the discontinuous system, and the model developed was validated by experimental results.

The major difference between an active and a passive impact was found to be in the case of low excitation amplitude where highly chaotic behavior was found from the grazing point. Interesting period incrementing cascades were also observed.

7.2 Impact oscillators – practical applications

The work presented in this thesis has profound effect on a lot of real life vibrating systems. It is possible due to incorrect design or dimensioning that systems

designed for linear vibrations may come in contact with another part in the assembly, and hence the response ends up being highly non-linear. This is quite detrimental to the life of the part which is designed for strength considering the linear FRF and hence is expected to have certain amplitude at a certain frequency. The most commonly used rule for design to minimize vibrations is to separate the natural frequency from the range of operating frequencies, so that the high amplitude at resonance is avoided.

However, as seen from the results presented in chapter 4,5 and 6 it is observed that the high amplitude vibrations exists for a much larger frequency range, and not only near resonance. Also, multiple solutions exist, which might result in erratic response of the system. It is possible that slight perturbations cause the system to move from one to another response. Hence, it is important to consider this nonlinear effect in real life design for systems that may potentially undergo imapct.

7.3 Scope for future work

The results obtained lead to a number of new topics to be determined in the case of impact oscillators, both theoretical and experimental. These are discussed in the following sections

7.3.1 Non-dimensionalized behavior

To get a better understanding of the expected type of response it is necessary to derive a relation between the position of the barrier, the excitation amplitude and the kick given to the system. For a passive impact, it is fairly obvious that for a constant ratio

of barrier position to excitation amplitude, changing the amplitude will result in the exact same qualitative behavior although on a different scale.

But the addition of the kick makes the relation more complicated. Hence it is necessary to repeat the experiments for different values of V. Experimentally this may be done by varying the voltage to the solenoid or by using a different solenoid of higher power. Ultimately, the two ratios which will govern the qualitative behavior for an active impact are: ratio of barrier location to forcing amplitude and ratio of solenoid kick to max velocity.

7.3.2 Basins of attraction

As a part of this research, numerical basins of attraction have been generated for both active and passive case. Interesting basins have been obtained including one with fractal basin boundaries. In chapter 7, hysteresis is observed for a region where chaotic and multiple period orbits co-exist, and the basins of attraction for such a case have been extensively studied and often have a highly fractal structure. As can be seen from chapter 7, there is a mismatch between the theoretical and experimental bifurcation diagrams. This could be because there are three co-existing attractors, and the theory and experimentation are picking up different ones. A study of the Initial Condition space will provide a better understanding of this behavior. We leave further exploration of the basins of attraction, both numerical and experimental as a topic for further research.

Stochastic Interrogation is a popular method to determine the experimental basins. This method consists of generating a random IC and then following the solution until it settles onto an attractor. In the case of the scotch yoke in the nonlinear dynamics lab, this can be done by switching off the power and then switching it back on to desired frequency to generate a set of ICs. The time for which the scotch yoke is switched off is decided by a random number generator.

7.3.3 Complicated models

The system analyzed here is a 1-D oscillating spring-mass- damper. Although the system is a simplistic treatment of a pinball machine, the behavior exhibited is quite rich and the analysis and experimentation are very complicated. The ultimate aim would be to analyze a 2D active impact oscillator with a magnetic bumper that has the freedom to move on a 2-D plane. The state space would be 4-dimensional instead of 2-dimensional. The impact in this case can also be complicated, since it is possible for the impact to be at an angle.

Appendix A

Gallery of Time series and Time Delay Plots

This appendix contains a collection of time series and time delay plots that correspond to interesting behavior displayed by the systems covered in chapters 4, 5 and 6. Each page contains 4 figures corresponding to the response to a certain excitation frequency and amplitude, a type of impact i.e. passive or active and either sweep up or sweep down. All figures on the left are numerical results whereas those on the right are experimental results.

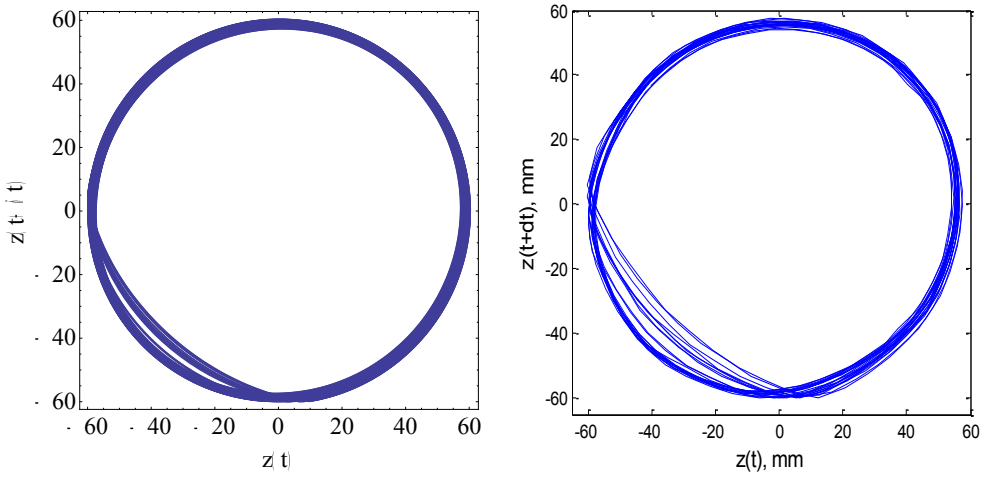

(a) Numerical state space (b) Experimental state space

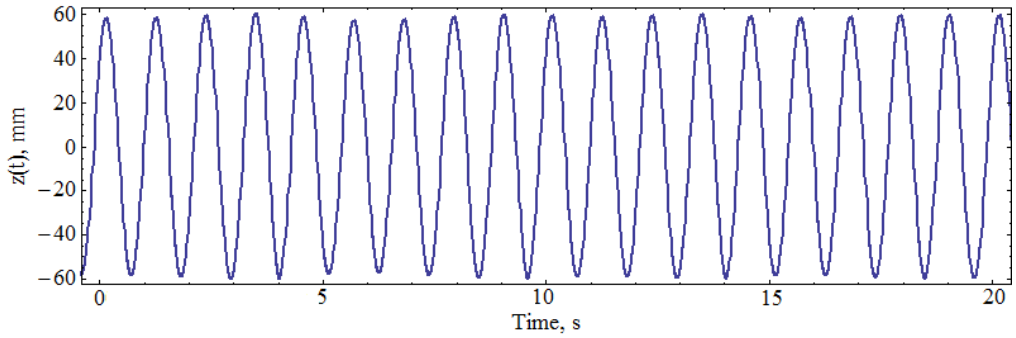

(c) Numerical time series

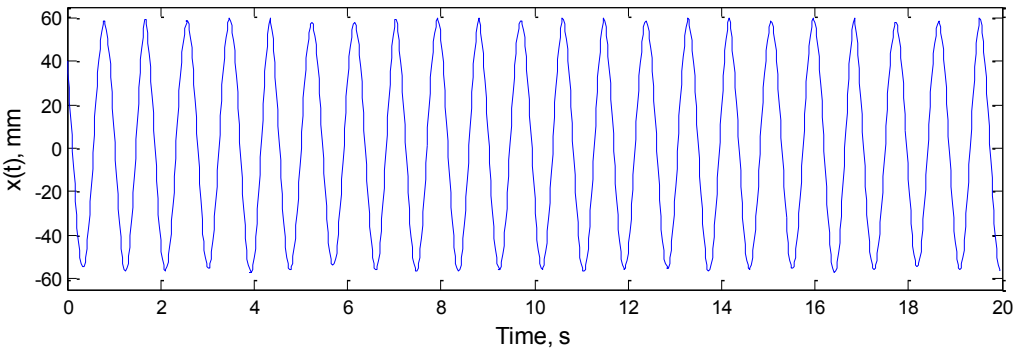

(d) Experimental time series

Figure 20. Results for ω=0.9 Hz, y_0=10 mm, passive impact, upsweep

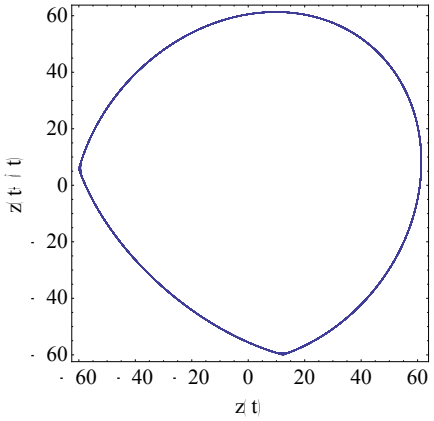

(a) Numerical state space

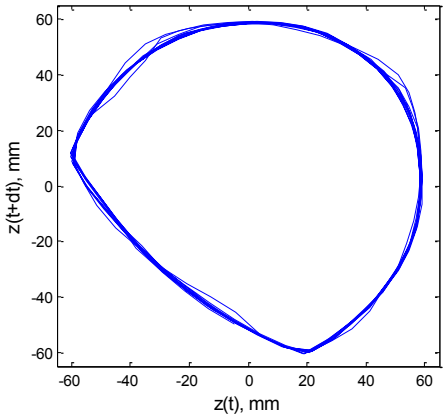

(b) Experimental state space

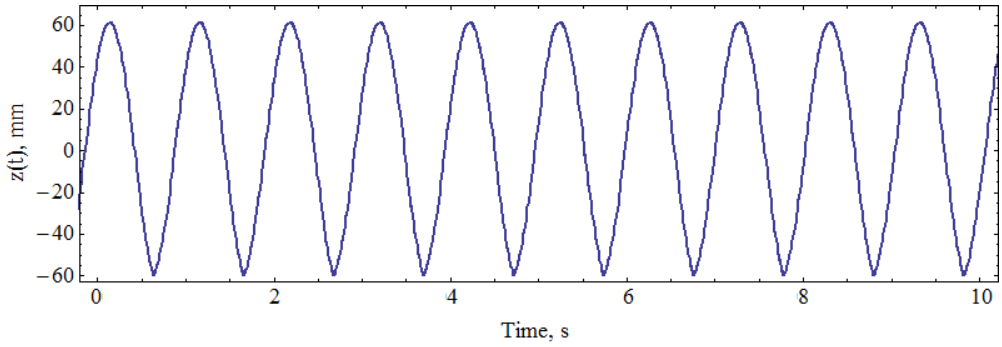

(c) Numerical time series

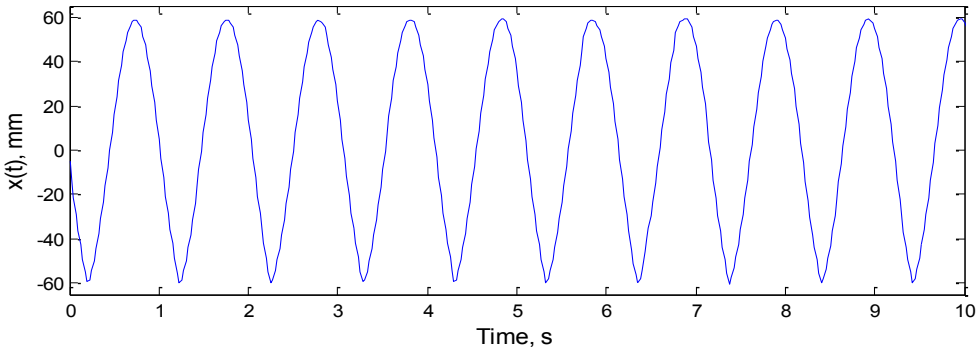

(d) Experimental time series

Figure 21. Results for ω=0.98 Hz, y_0=10 mm, passive impact, upsweep

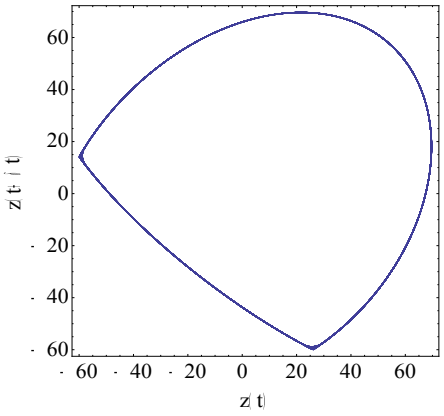

(a) Numerical state space

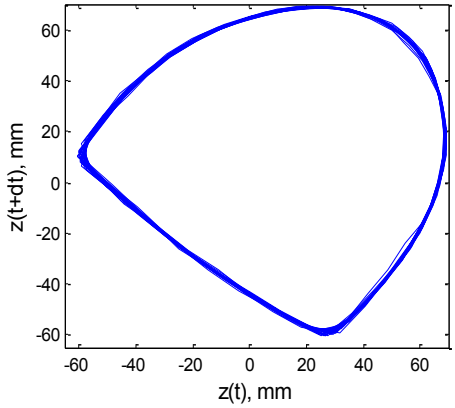

(b) Experimental state space

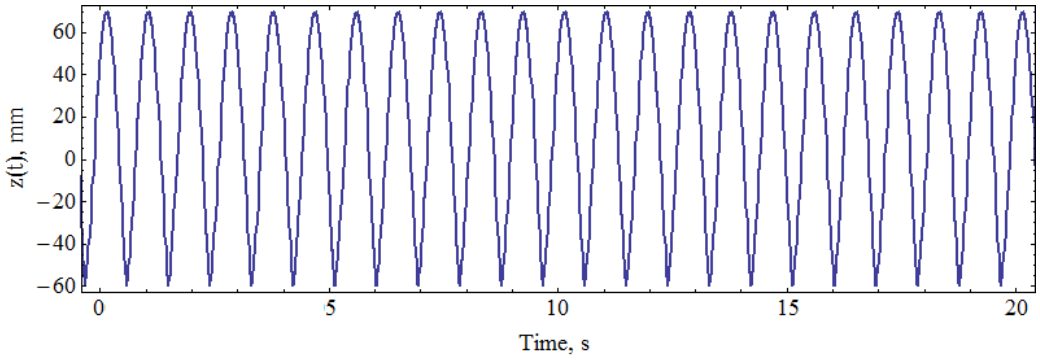

(c) Numerical time series

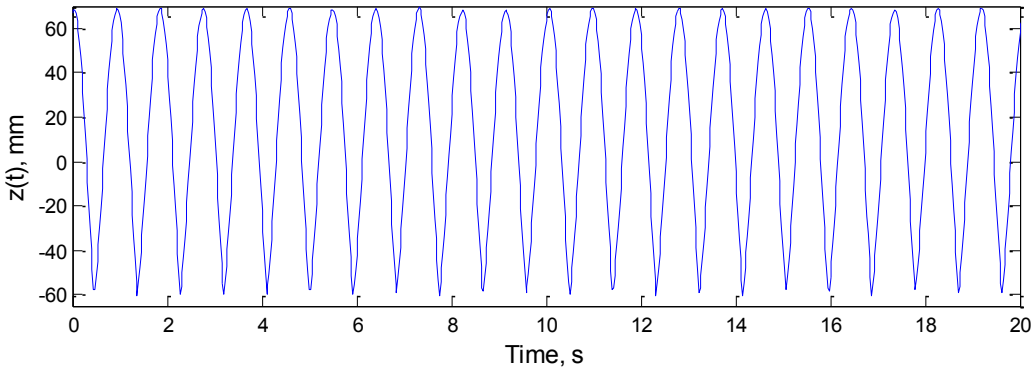

(d) Experimental time series

Figure 22. Results for ω=1.1 Hz, y_0=10 mm, passive impact, upsweep

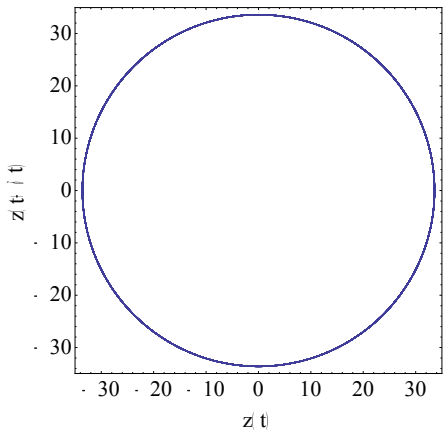

(a) Numerical state space

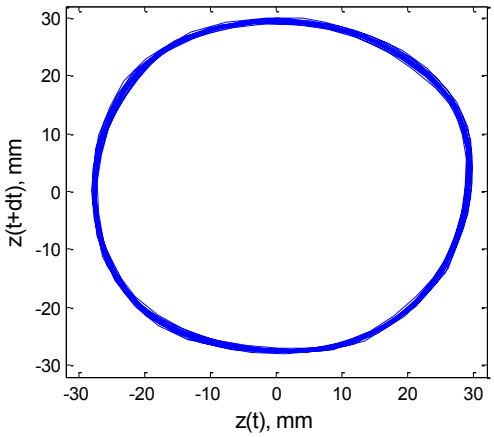

(b) Experimental state space

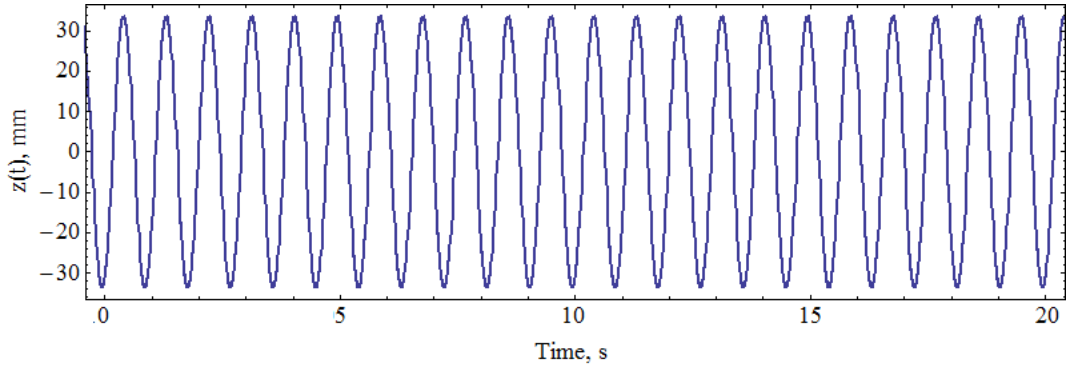

(c) Numerical time series

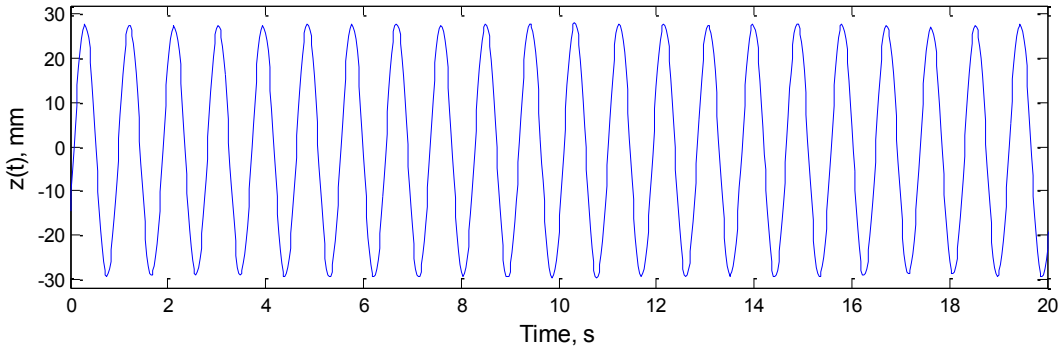

(d) Experimental time series

Figure 23. Results for ω=1.1 Hz, y0=10 mm, passive impact, downsweep

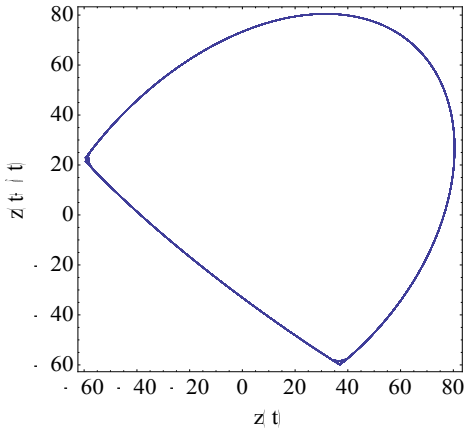

(a) Numerical state space

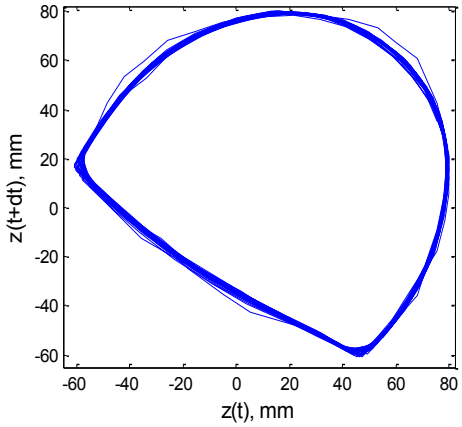

(b) Experimental state space

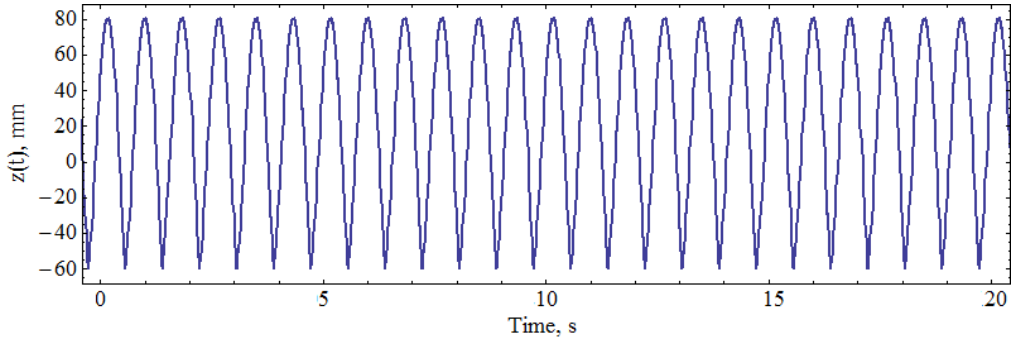

(c) Numerical time series

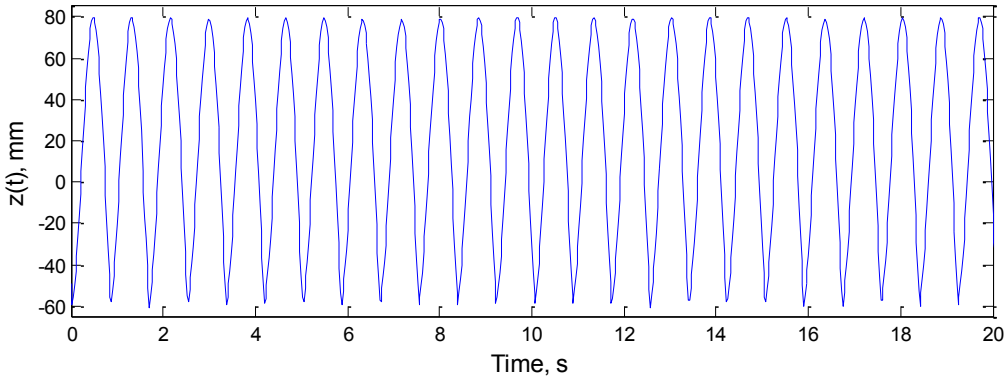

(d) Experimental time series

Figure 24. Results for ω=1.2 Hz, y0=10 mm, passive impact, upsweep

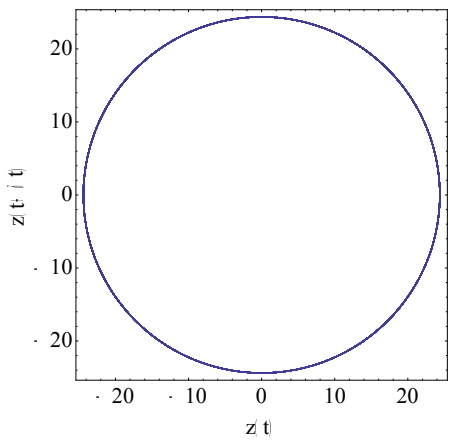

(a) Numerical state space

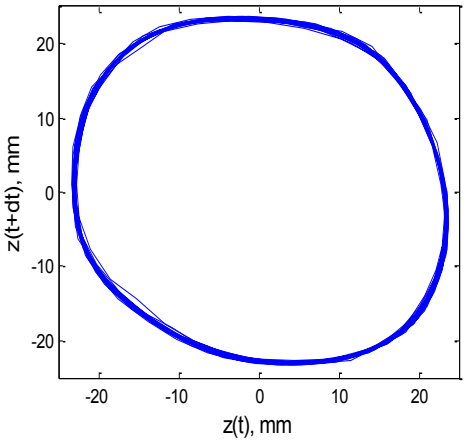

(b) Experimental state space

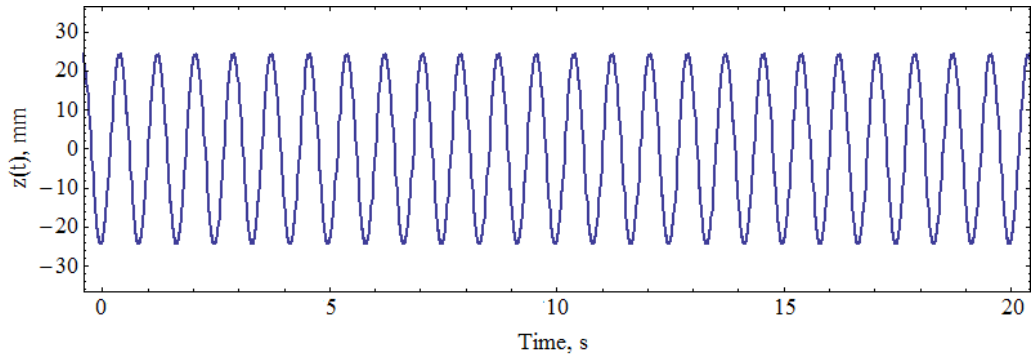

(c) Numerical time series

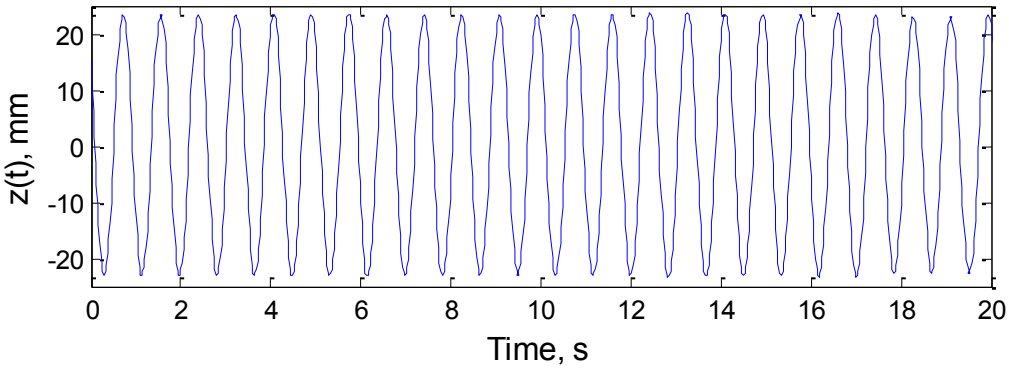

d) Experimental time series

Figure 25. Results for ω=1.2 Hz, y0=10 mm, passive impact, downsweep

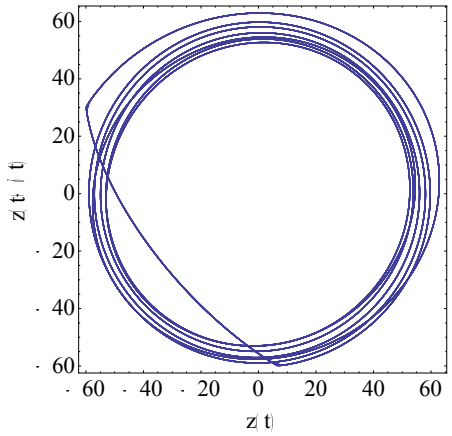

(a) Numerical state space

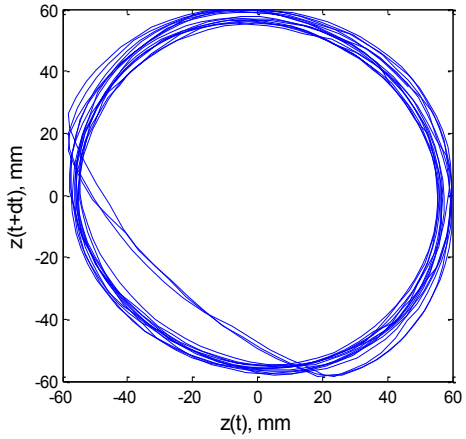

(b) Experimental state space

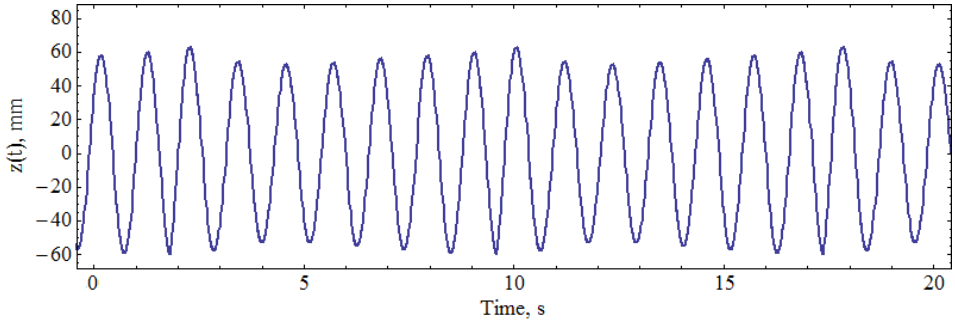

(c) Numerical time series

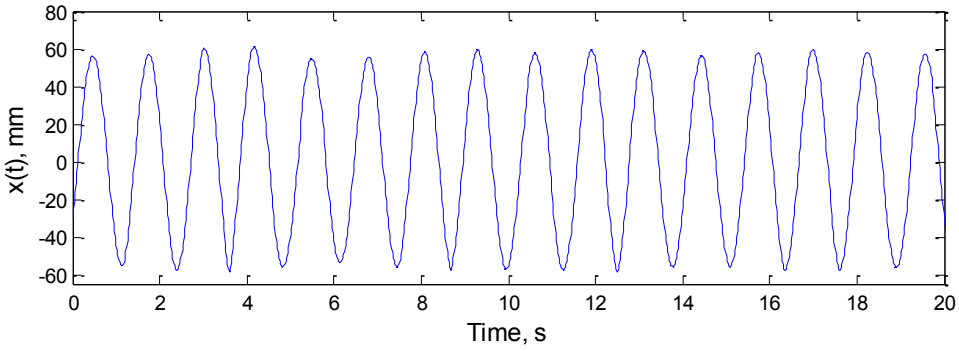

d) Experimental time series

Figure 26. Results for ω=0.9 Hz, y0=10 mm, active impact, up sweep

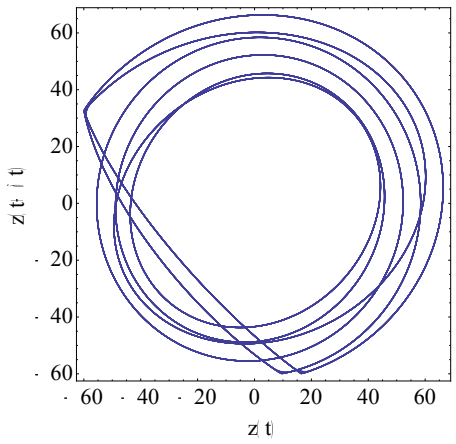

(a) Numerical state space

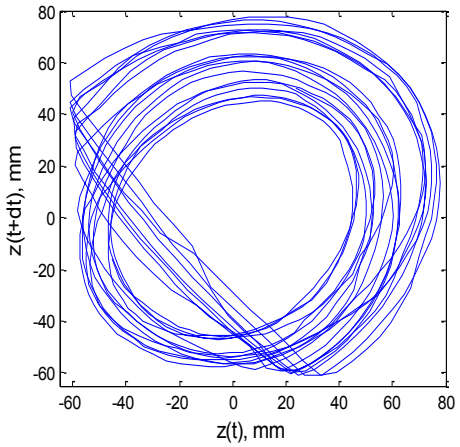

(b) Experimental state space

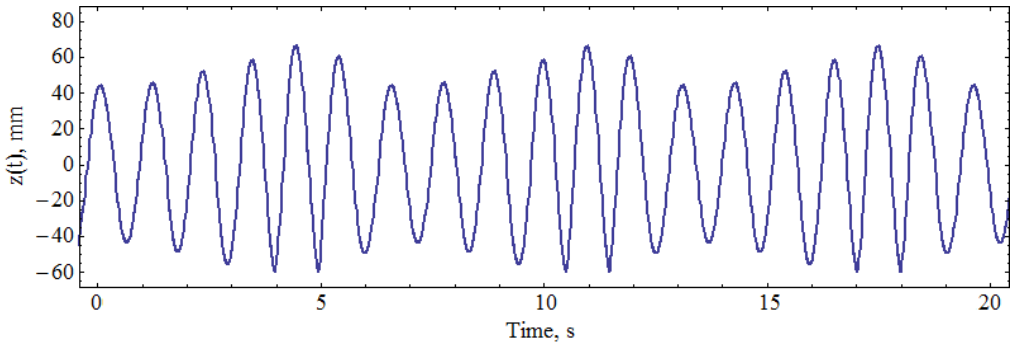

(c) Numerical time series

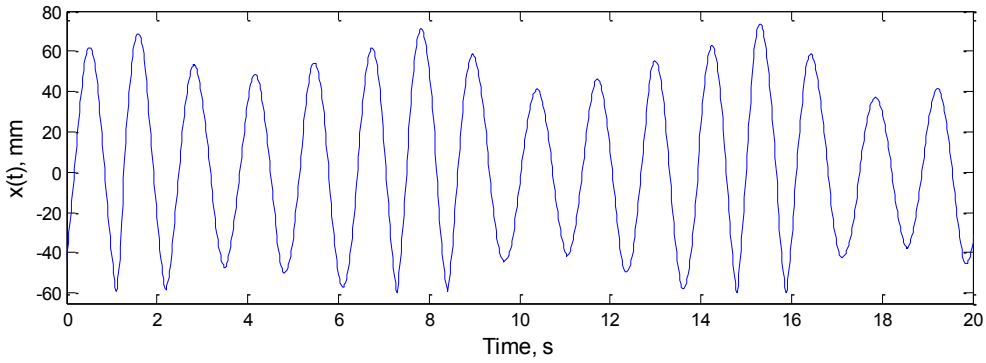

d) Experimental time series

Figure 27. Results for ω=0.92 Hz, y0=10 mm, active impact, up sweep

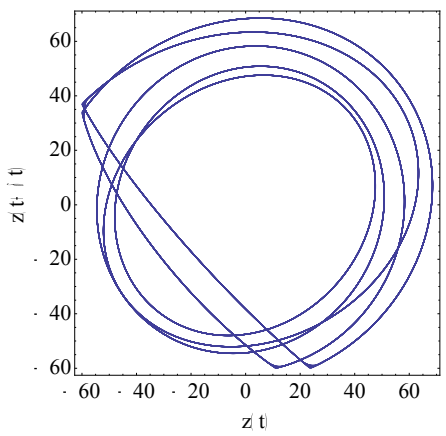

(a) Numerical state space

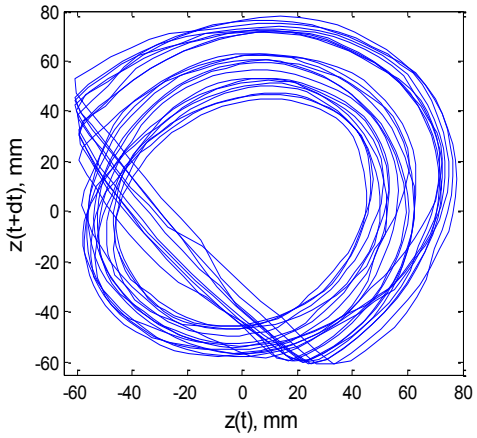

(b) Experimental state space

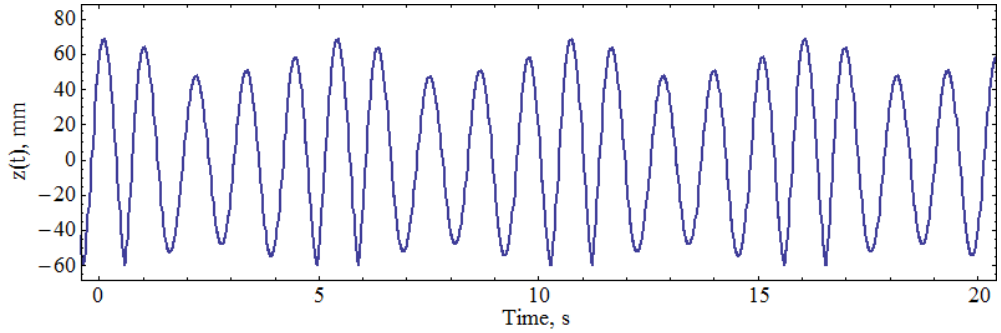

(c) Numerical time series

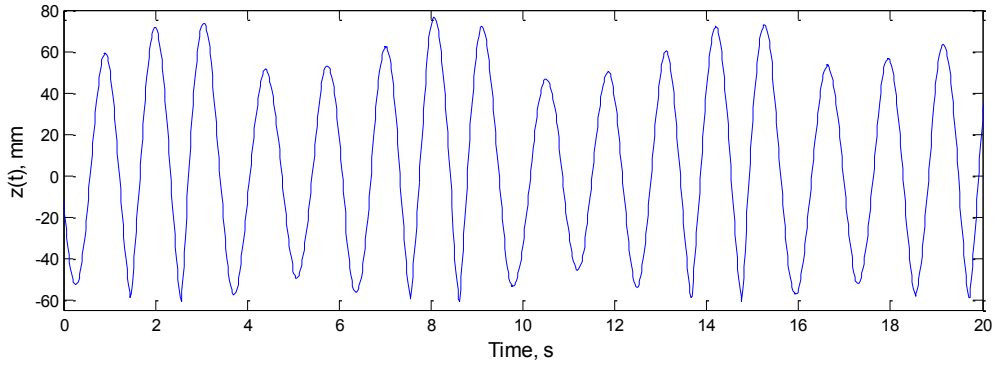

d) Experimental time series

Figure 28. Results for ω=0.94 Hz, y0=10 mm, active impact, up sweep

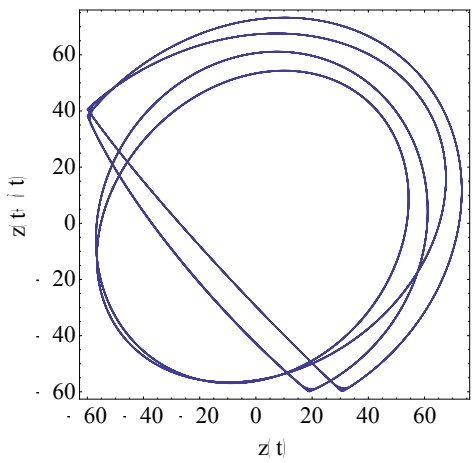

(a) Numerical state space

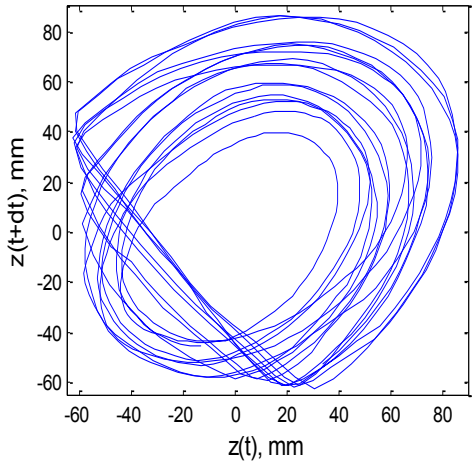

(b) Experimental state space

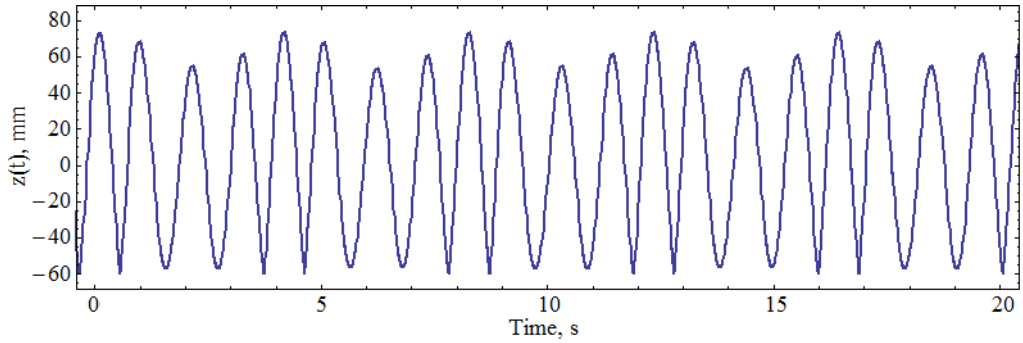

(c) Numerical time series

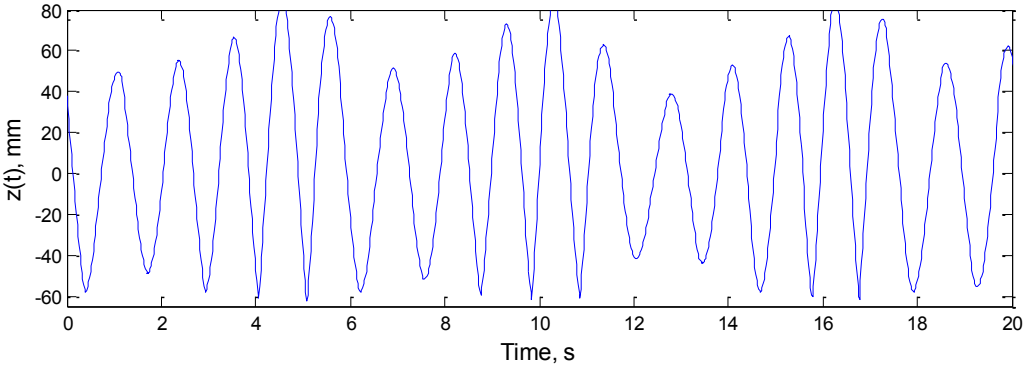

d) Experimental time series

Figure 29. Results for ω=0.98 Hz, y0=10 mm, active impact, up sweep

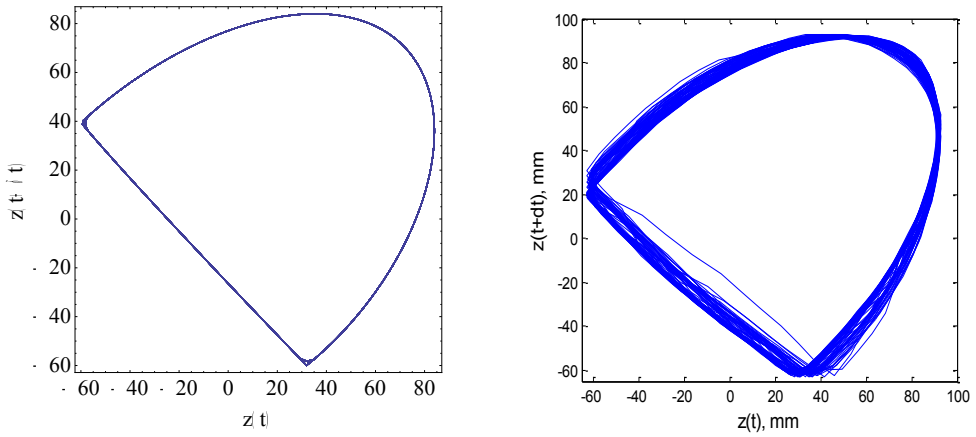

(a) Numerical state space (b) Experimental state space

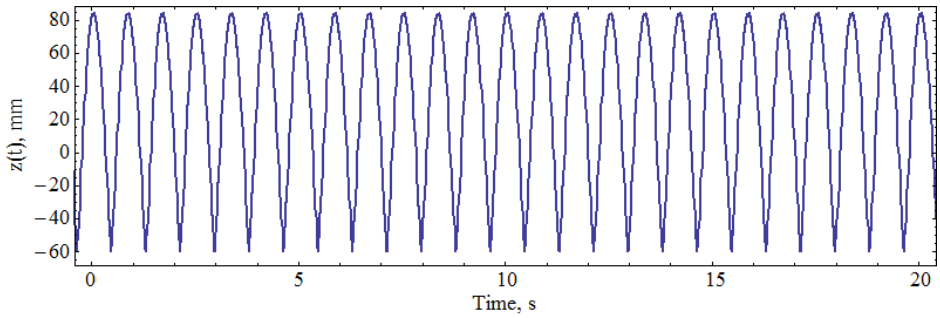

(c) Numerical time series

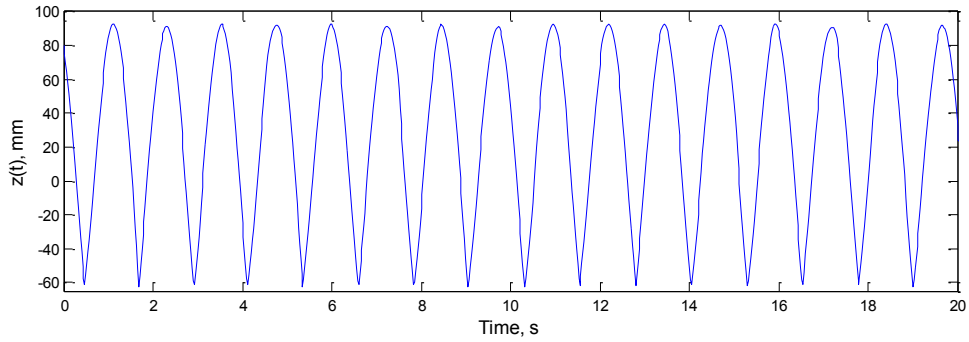

d) Experimental time series

Figure 30. Results for ω=1.2 Hz, y0=10 mm, active impact, up sweep

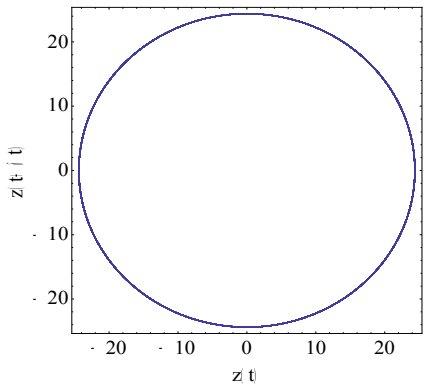

(a) Numerical state space

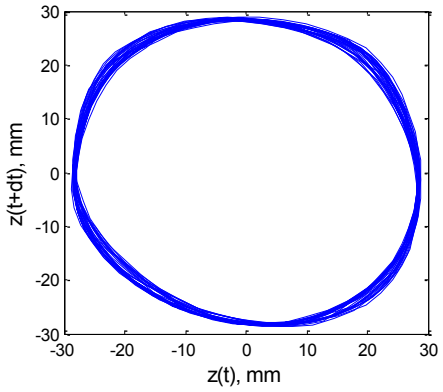

(b) Experimental state space

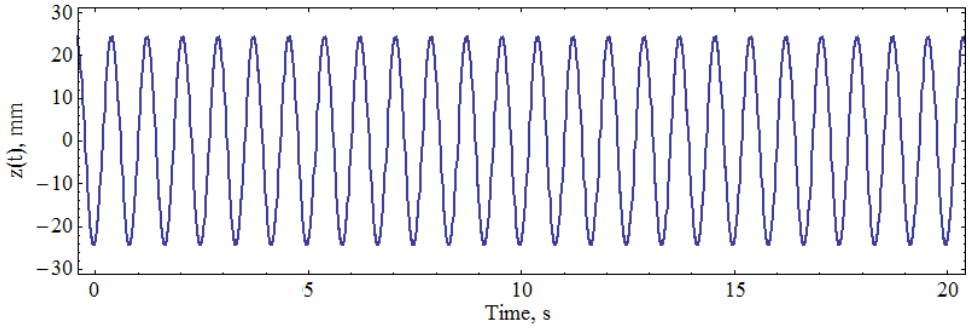

(c) Numerical time series

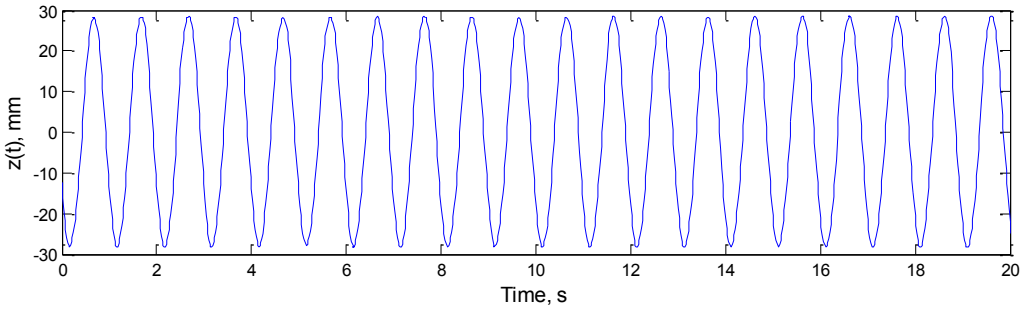

d) Experimental time series

Figure 31. Results for ω=1.2 Hz, y0=10 mm, active impact, down sweep

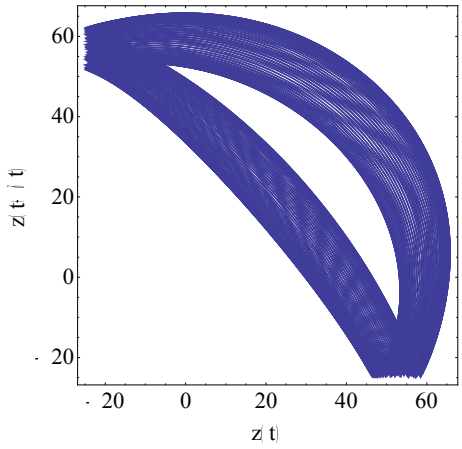

(a) Numerical state space

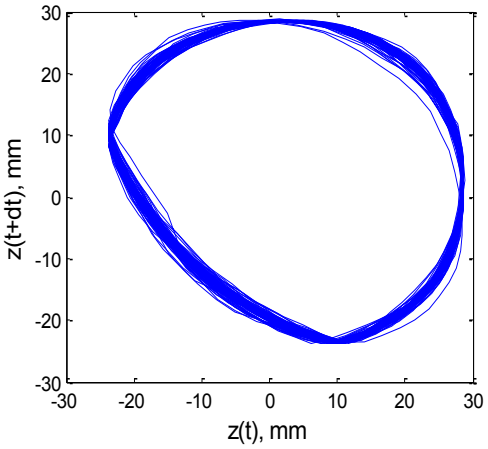

(b) Experimental state space

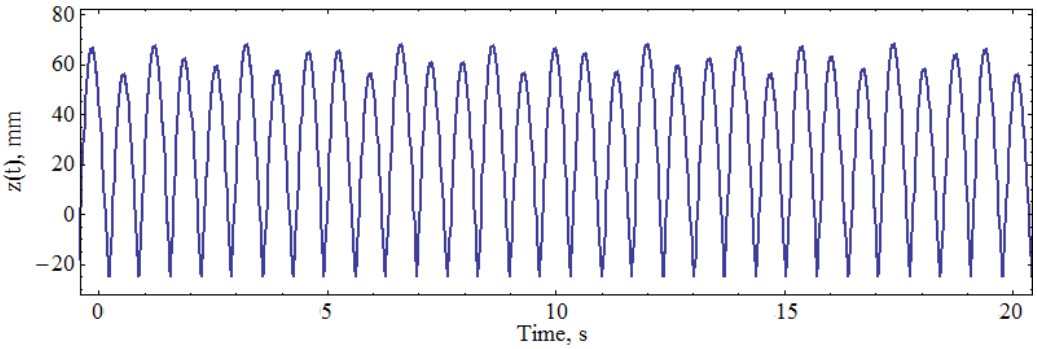

(c) Numerical time series

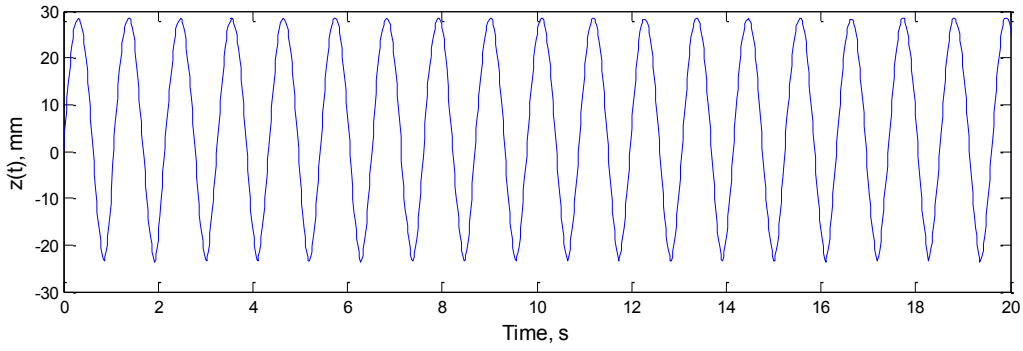

d) Experimental time series

Figure 32. Results for ω=0.92 Hz, y0=7 mm, active impact, up sweep

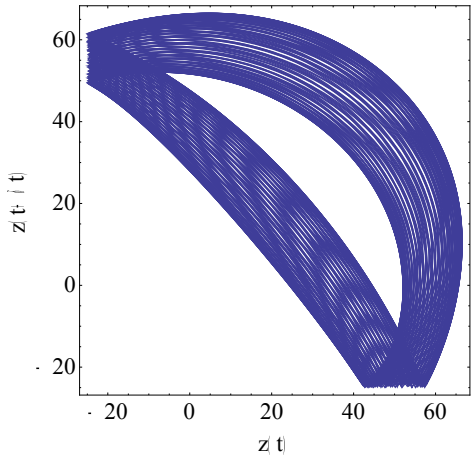

(a) Numerical state space

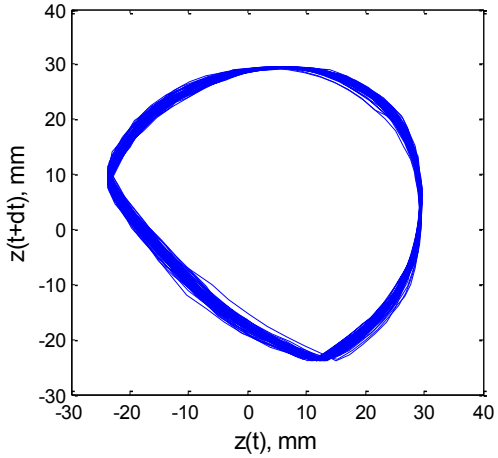

(b) Experimental state space

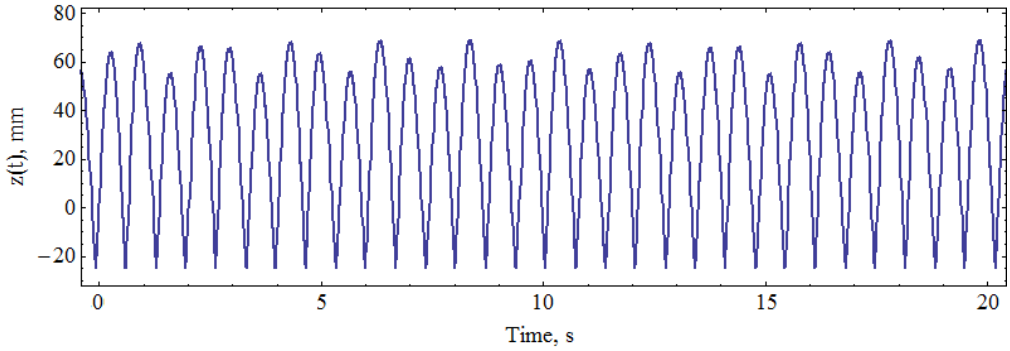

(c) Numerical time series

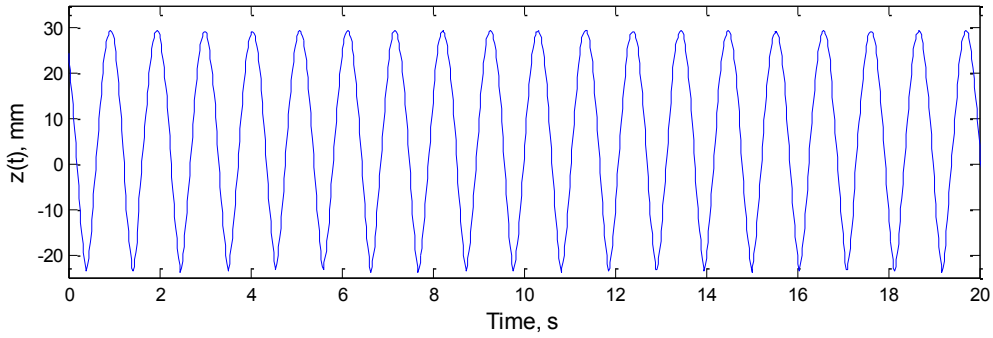

d) Experimental time series

Figure 33. Results for ω=0.96 Hz, y0=7 mm, active impact, up sweep

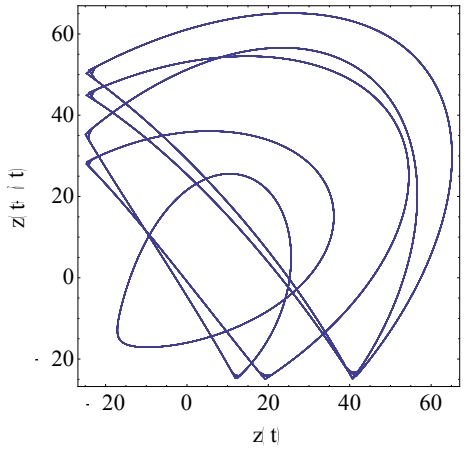

(a) Numerical state space

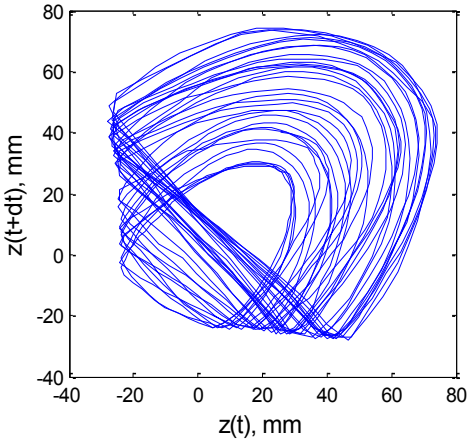

(b) Experimental state space

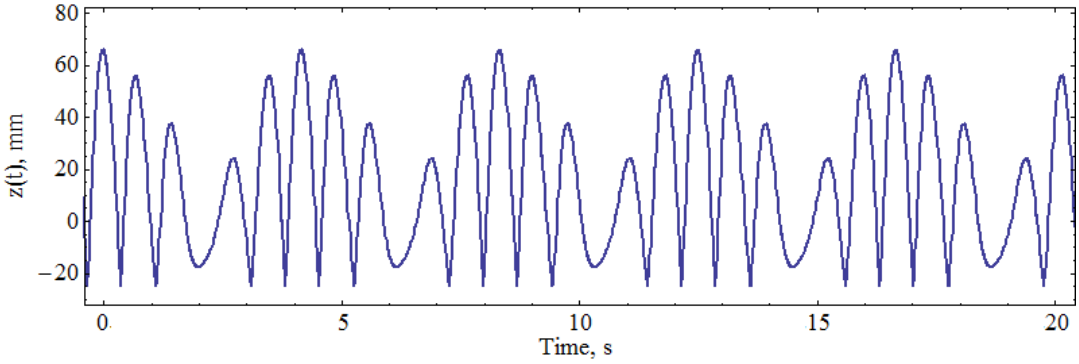

(c) Numerical time series

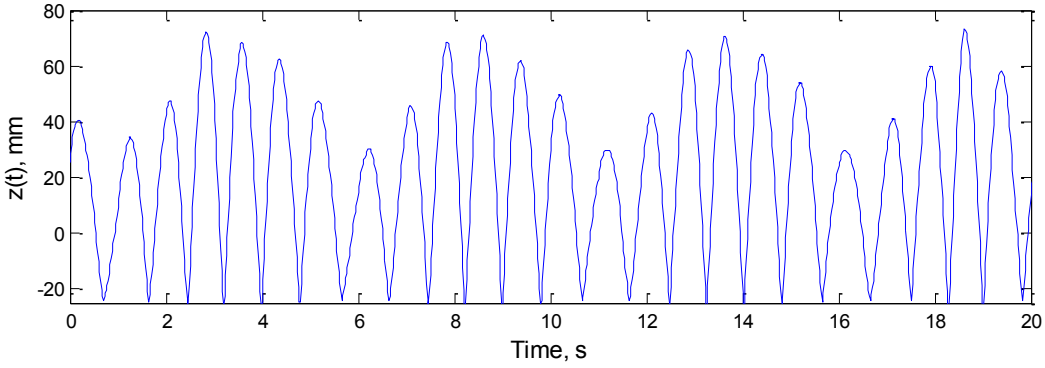

d) Experimental time series

Figure 34. Results for ω=1.2 Hz, y0=7 mm, active impact, up sweep

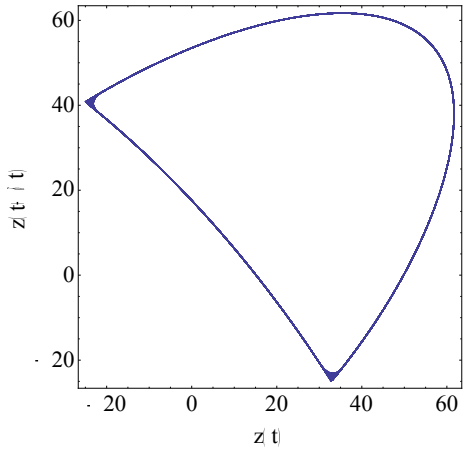

(a) Numerical state space

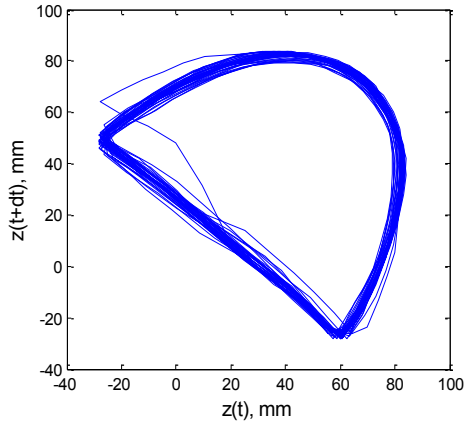

(b) Experimental state space

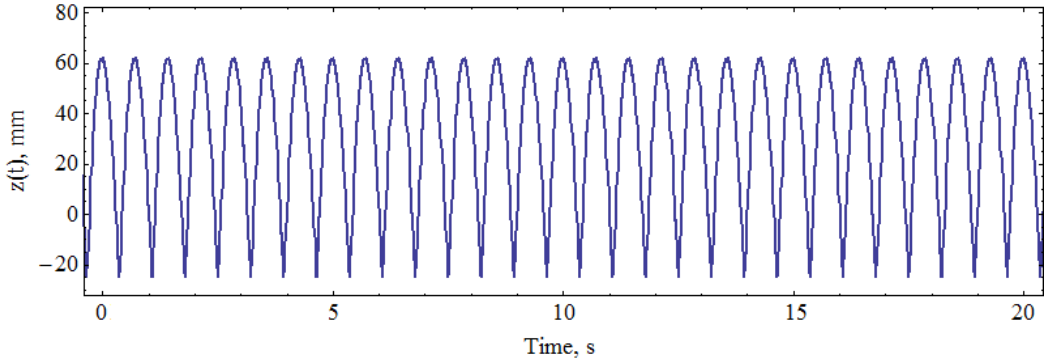

(c) Numerical time series

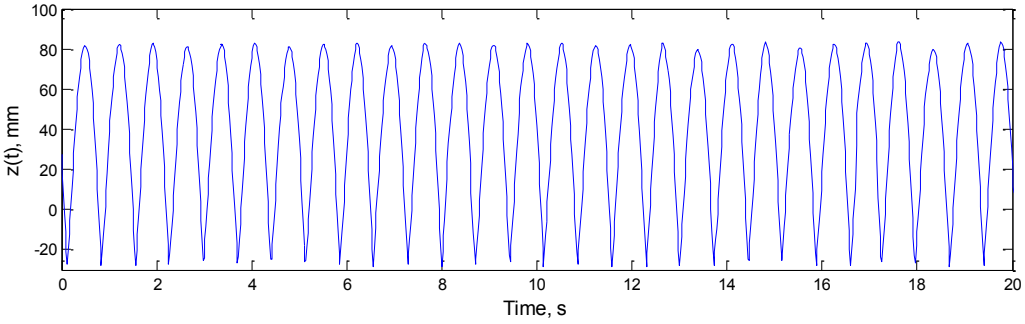

d) Experimental time series

Figure 35. Results for ω=1.4 Hz, y0=7 mm, active impact, up sweep

Appendix B

Gallery of Poincaré Sections

This section displays the Poincaré section obtained by numerical simulations for some of the interesting behavior observed in chapters 6, 7 and 8. The Poincaré sections shown are in time-delayed coordinates with a quarter lag delay, similar to the state space plotted in Appendix 1.

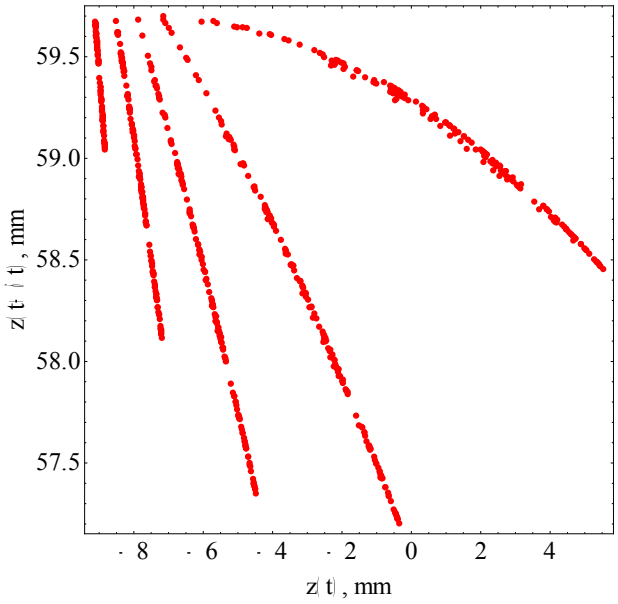

Figure 36. Poincaré section for ω=0.9 Hz, y0=10 mm, passive impact – taken at grazing point

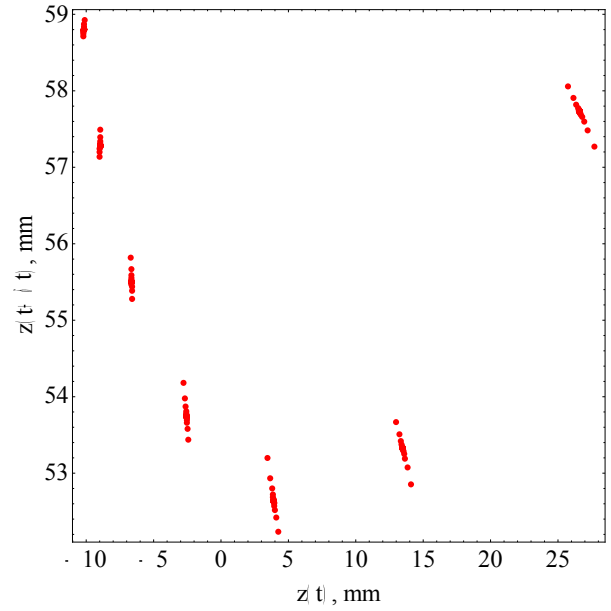

Figure 37. Poincaré section for ω=0.9 Hz, y0=10 mm, barrier = -60 mm, active impact – taken at grazing point

Bibliography

[1] Nordmark, A.B. (1991) *Non-periodic motion caused by grazing incidence in an impact oscillator*, Journal of Sound and Vibration, 145, 279-297.

[2] Peterka, F. and Vacik, J. (1992) *Transition to Chaotic Motion in Mechanical Systems with Impacts,* Journal of Sound and Vibrations, 154, 95-115.

[3] Nordmark, A. B. (1992*), Effects Due to Low Velocity Impact in Mechanical Oscillators*, International Journal of Bifurcation and Chaos, 2, 597-605.

[4] Thompson, J.M.T and Ghaffari, R. (1983) *Chaotic Dynamics of an Impact Oscillator,* Physical Review A, 27, 1741-1743.

[5] Strogatz, S.H. (1994) *Introduction to Nonlinear Dynamics,* Addison Wesley Publishing Company.

[6] Piiroinen, P.T., Virgin, L.N. and Champneys, A.R. (2004) *Chaos and Period-Adding; Experimental and Numerical Verification of the Grazing Bifurcation,* Journal of Nonlinear Science, 14, 383-404.

[7] Bayly, P.V. and Virgin, L.N. (1993) *An Experimental Study of an Impacting Pendulum,* Journal of Sound and Vibration, 364–374.

[8] Davis, R.B. and Virgin, L.N. (2007) *Non-linear behavior in a discretely forced oscillator,* International Journal of Non-Linear Mechanics 42, 744 -753.

[9] Pring, S.R. and Budd, C.J. (2011) *The dynamics of a simplified pinball machine*, IMA Journal of Applied Mathematics, 76, 67-84.

[10] Shaw, S.W. & Holmes P.J. (1983) *A periodically forced piecewise linear oscillator,* Journal of Sound and Vibration, 90, 129-155.

[11] Virgin, L. N. (2000), *Introduction to Experimental Nonlinear Dynamics*, Cambridge University Press.